This peer-reviewed published paper appears as: Hwang, S.-H., Lignos, D.G. (2017). "Effect of Modeling Assumptions on the Earthquake-Induced Losses and Collapse Risk of Steel-Frame Buildings with Special Concentrically Braced Frames", *Journal of structural Engineering*, **143**(9), 04017116-1, DOI:10.1061/(ASCE)ST.1943-541X.0001851.

Effect of Modeling Assumptions on the Earthquake-Induced Losses and Collapse Risk of Steel-Frame Buildings with Special Concentrically Braced Frames

Seong-Hoon Hwang[1]

Dimitrios G. Lignos, A.M. ASCE[2]

ABSTRACT

This paper quantifies the collapse risk and earthquake-induced economic losses of steel-frame buildings with special concentrically braced frames designed in urban California. A probabilistic building-specific loss estimation methodology that can explicitly account for the main sources of variability related to seismic hazards and structural response is utilized for this purpose. It is shown that, depending on the choice of the loss-metric, at seismic events with low probability of occurrence (i.e., 2% probability of occurrence in 50 years), losses because of demolition and structural collapse in steel-frame buildings with special concentrically braced frames designed in highly seismic zones may be significantly overestimated when ignoring the contribution of the composite floor and gravity framing system to the analytical model building representation. For frequent and moderately frequent seismic events (i.e., 50 and 10% probability of exceedance over 50 years of building life expectancy), acceleration-sensitive nonstructural component repairs govern building losses regardless of the analytical model representation used. For the same seismic events, an appreciable contributor to total losses in steel-frame buildings with special concentrically braced

[1]Graduate Student, Dept. of Architecture, Civil and Environmental Engineering, Swiss Federal Institute of Technology, École Polytechnique Fédérale de Lausanne, EPFL ENAC IIC RESSLab, CH-1015 Lausanne, Switzerland; Dept. of Civil Engineering and Applied Mechanics, McGill Univ., Montreal, QC, Canada H3A 2K6. E-mail: seong-hoon. hwang@epfl.ch, seong-hoon.hwang@mail.mcgill.ca

[2]Associate Professor, Dept. of Architecture, Civil and Environmental Engineering, Swiss Federal Institute of Technology, École Polytechnique Fédérale de Lausanne, EPFL ENAC IIC RESSLab, CH-1015 Lausanne, Switzerland (corresponding author). E-mail: dimitrios.lignos@epfl.ch.

frames is structural repairs because of steel brace flexural buckling. It is suggested that dual-parameter rather than drift-based steel brace fragility curves should be used in loss computations conditioned on a single seismic intensity. Otherwise, the expected annual losses should be used as a metric for building-specific loss assessment of steel-frame buildings with special concentrically braced frames.

Keywords: Earthquake loss assessment; Collapse risk; Special concentrically braced frames; Losses because of demolition; Gravity framing; residual deformations; Seismic effects.

INTRODUCTION

Steel concentrically braced frames (CBFs) are a widely used lateral load-resisting system around the world to withstand earthquake loading. Because of the steel brace's asymmetric hysteretic behavior in combination with a wide-range of CBF configurations, local story collapse mechanisms may develop because of plastic deformation concentrations. This could potentially result into large residual story deformations or structural collapse (Tremblay et al. 1995; Tremblay et al. 1996). The magnitude of residual deformations along the height of a building is likely to affect decisions associated with building demolition in the aftermath of an earthquake (Ramirez and Miranda 2012). During more frequently occurring earthquakes (i.e., service-level or design-basis earthquakes), steel CBFs may experience fairly high absolute acceleration demands because of the high lateral stiffness they can provide compared to other lateral load-resisting systems as well as the contribution of higher mode effects to the structural response (Rodriguez et al. 2002; Chopra 2011; Ray-Chaudhuri and Hutchinson 2011). Prior studies (Tremblay 2002; Roeder et al. 2012; Lignos and Karamanci 2013) have indicated that steel brace flexural buckling typically occurs, on average, at a story drift ratio (i.e., the ratio of the relative lateral displacement between two adjacent floors to the story height) of approximately 0.5%. Considering all the previous, steel CBFs may experience appreciable earthquake-induced losses because of damage in the structural and nonstructural building content at seismic intensities associated with design-basis earthquakes. Such losses should be quantified in a rational manner.

With the advent of performance-based earthquake engineering (PBEE) (Cornell and Krawinkler 2000; FEMA 2012), a number of studies quantified earthquake-induced losses mainly for conventional reinforced concrete (Mitrani-Reiser 2007; Ramirez et al. 2012; Baradaran Shoraka et al. 2013) and wood structures (Porter et al. 2006; Pei and van de Lindt 2009). In a more recent study, Song et al. (2016) showed that the earthquake-induced losses of steel-frame buildings accounting for mainshock-aftershock sequences are approximately 27–40% higher than those considering mainshocks only. Ramirez and Miranda (2012) pointed out that building demolition may become a controlling parameter in conventional modern building construction because of large residual deformations. Liel and Deierlein (2013) showed that direct earthquake-induced losses in nonductile reinforced concrete buildings are only twice those for modern code-compliant buildings, whereas their collapse risk is on the order of at least 30 times higher than code-conforming buildings. To the best of the authors' knowledge, there has not been an attempt to quantify the structural and nonstructural repairs needed in steel-frame buildings with CBFs in the aftermath of an earthquake. This process is not trivial because it should explicitly consider the beneficial influence of gravity framing and column continuity on the distribution of story drift demands and reserve capacity of the steel-frame buildings (Gupta and Krawinkler 1999; MacRae et al. 2004; Ji et al. 2009; Stoakes and Fahnestock 2011; Fahnestock et al. 2014; Flores et al. 2014; Elkady and Lignos 2015; Flores et al. 2016); else, the estimated economic losses can be vastly overestimated (NIST 2012b).

Building-specific loss estimation methodologies are typically based on univariate (i.e., either drift- or acceleration-based) fragility curves for structural and nonstructural building components (Porter et al. 2001; FEMA 2012; Li and van de Lindt 2012). This is done in an effort to retain simplicity in the loss computations. However, damageable components may be very sensitive to other geometric and material parameters that are often ignored as part of the loss estimation process. Aslani and Miranda (2005) demonstrated that bivariate fragility curves are more suitable than drift-based fragilities to characterize slab-column connection damage in existing nonductile reinforced concrete buildings. In a more recent study, Lignos and Karamanci (2013) demonstrated the efficiency of dual-parameter fragility curves for building-specific loss estimation of steel CBFs. This is because of the influence of steel brace global and local slenderness on the predefined steel brace damage states that are used within the current loss estimation methodologies.

This paper addresses all the aforementioned issues by evaluating the expected earthquake-induced losses in archetype steel-frame buildings with special concentrically braced frames (SCBFs) designed in urban California. The evaluation is conducted at various ground motion intensities until the occurrence of structural collapse. In this process, the influence of residual deformations on the building repairs is explicitly considered. Emphasis is placed on the effect of gravity framing and the selected steel brace fragility curve on the loss computations. The influence of the selected seismic design category on the earthquake-induced losses of steel-frame buildings with SCBFs is examined. Guidance on the selection of the appropriate loss-metric is also provided, depending on the seismic performance of interest.

OVERVIEW OF SEISMIC LOSS ESTIMATION METHODOLOGY USED

The main aspects of the used building-specific loss estimation methodology adopted from Ramirez and Miranda (2012) are summarized herein. This is a story-based building-specific loss estimation methodology in which engineering demand parameters (EDPs) at each story are computed based on nonlinear response history analysis. The methodology described below has been implemented in an interactive *MATLAB* routine (MATLAB 2015). By assuming mutually exclusive and collectively exhaustive events of building collapse and no collapse, the mean of total seismic losses in a frame building conditioned on the seismic intensity measure IM=*im* (i.e., $\mu_{L_T|\mathrm{IM}}$) is described by,

$$\mu_{L_T|\mathrm{IM}} = \mu_{L_{\mathrm{NC}}|\mathrm{IM,NC}} \left(1 - P_{C|\mathrm{IM}}\right) + \mu_{L_C|C} P_{C|\mathrm{IM}} \quad (1)$$

where $\mu_{L_{\mathrm{NC}}|\mathrm{IM,NC}}$ is the mean value of the loss conditioning on no collapse for a given IM=*im*; $\mu_{L_C|C}$ is the mean value of the loss because of collapse (this is independent of seismic intensity IM); and $P_{C|\mathrm{IM}}$ is the collapse probability given an IM=*im*. Non-collapse losses $\mu_{L_{\mathrm{NC}}|\mathrm{IM,NC}}$ can be further disaggregated into losses because of repairs for structural, drift-sensitive, acceleration-sensitive nonstructural components and demolition as discussed in Ramirez and Miranda (2012).

Therefore, Eq. (1) can be rewritten as,

$$\mu_{L_T|\mathrm{IM}} = \mu_{L_R|R,\mathrm{IM,NC}} P_{R|\mathrm{IM,NC}} \left(1 - P_{C|\mathrm{IM}}\right) + \mu_{L_D|D,\mathrm{IM,NC}} P_{D|\mathrm{IM,NC}} \left(1 - P_{C|\mathrm{IM}}\right) + \mu_{L_C|C} P_{C|\mathrm{IM}} \quad (2)$$

where $\mu_{L_R|R,\mathrm{IM,NC}}$ is the mean of losses because of repairs for structural and nonstructural components conditioned on no collapse given a seismic intensity IM=*im*; $\mu_{L_D|D,\mathrm{IM,NC}}$ is the mean of losses because of demolition conditioned on no collapse, given a seismic intensity IM=*im*; $P_{R|\mathrm{IM,NC}}$ and $P_{D|\mathrm{IM,NC}}$ are the probabilities that the building is being considered to be repaired and be demolished, respectively, both conditioned on no collapse given a seismic intensity IM=*im*; therefore, Eq. (2) becomes,

$$\mu_{L_T|\mathrm{IM}} = \mu_{L_R|R,\mathrm{IM,NC}} \left(1 - P_{D|\mathrm{IM,NC}}\right) \left(1 - P_{C|\mathrm{IM}}\right) + \mu_{L_D|D,\mathrm{IM,NC}} P_{D|\mathrm{IM,NC}} \left(1 - P_{C|\mathrm{IM}}\right) + \mu_{L_C|C} P_{C|\mathrm{IM}} \quad (3)$$

In this paper, $\mu_{L_R|R,\mathrm{IM,NC}}$ can be estimated by considering the discrete damage state a component experiences by using Eq. (4),

$$\mu_{L_R|R,\mathrm{IM,NC}} = \sum_{i=1}^{m} \sum_{j=0}^{n} \int_0^\infty \mu_{L_{ij}|\mathrm{DS}_{ij}} P_{\mathrm{DS}_{ij}|\mathrm{EDP}} f_{\mathrm{EDP}|IM} \, d\mathrm{EDP} \quad (4)$$

where *m* is the number of damageable components being considered; *n* is the number of damage states a component may experience; $\mu_{L_{ij}|\mathrm{DS}_{ij}}$ is the mean repair cost for the *i*th component being in the *j*th damage state; $P_{\mathrm{DS}_{ij}|\mathrm{EDP}}$ is the probability of the EDP of interest associated with the *i*th component being or exceeding the *j*th damage state given an EDP=*edp*,

$$P_{\mathrm{DS}_{ij}|\mathrm{EDP}} = \begin{cases} 1 - F_{\mathrm{DS}_{i1}}(\mathrm{EDP}) & \text{if } j = 0 \,(\text{no damage}) \\ F_{\mathrm{DS}_{ij}}(\mathrm{EDP}) - F_{\mathrm{DS}_{i(j+1)}}(\mathrm{EDP}) & \text{if } 1 \le j < n \\ F_{\mathrm{DS}_{ij}}(\mathrm{EDP}) & \text{if } j = n \end{cases} \quad (5)$$

where $F_{\mathrm{DS}_{ij}}$ is the fragility curve for the *i*th component being in the *j*th damage state, that is the probability that the component of being or exceeding damage state *ds* conditioned on an EDP=*edp* of interest; and $f_{\mathrm{EDP}|\mathrm{IM}}$ is the probability density function of the EDP of interest given an IM=*im*.

In the case in which dual-parameter fragility curves are used for a structural component (e.g., steel brace in this case) as part of the PBEE framework, Eq. (5) should be modified as follows in order to take into account both the EDP and the considered geometric parameter (GP) of the respective structural component,

$$P_{\mathrm{DS}_{ij}|\mathrm{EDP,GP}} = \begin{cases} 1 - F_{\mathrm{DS}_{i1}}(\mathrm{EDP,GP}) & \text{if } j = 0 \,(\text{no damage}) \\ F_{\mathrm{DS}_{ij}}(\mathrm{EDP,GP}) - F_{\mathrm{DS}_{i(j+1)}}(\mathrm{EDP,GP}) & \text{if } 1 \leq j < n \\ F_{\mathrm{DS}_{ij}}(\mathrm{EDP,GP}) & \text{if } j = n \end{cases} \tag{6}$$

where $P_{\mathrm{DS}_{ij}|\mathrm{EDP,GP}}$ is the fragility curve of the structural component being in the *j*th damage state, *ds* conditioned on the EDP=*edp* and the geometric parameter GP=*gp* of interest; $F_{\mathrm{DS}_{ij}}(\mathrm{EDP, GP})$ is the fragility curve that computes the probability of being or exceeding the *j*th damage state of the *i*th structural component conditioned on the EDP=*edp* and the geometric parameter GP=*gp* of interest (e.g., global or local slenderness). If the two random variables (i.e., EDP and *GP*) are lognormally distributed, a joint probability distribution $F_{\mathrm{DS}_{ij}}(\mathrm{EDP, GP})$ may be represented by a bivariate lognormal distribution (Aitchison and Brown 1957). For steel braces, it was found that the random variables of the dual-parameter fragility curves are statistically independent (Lignos and Karamanci 2013); therefore, Eq. (6) is modified as follows,

$$P_{\mathrm{DS}_{ij}|\mathrm{EDP,GP}} = \begin{cases} 1 - F_{\mathrm{DS}_{i1}}(\mathrm{EDP})\, F_{\mathrm{DS}_{i1}}(\mathrm{GP}) & \text{if } j = 0 \,(\text{no damage}) \\ F_{\mathrm{DS}_{ij}}(\mathrm{EDP})\, F_{\mathrm{DS}_{ij}}(\mathrm{GP}) - F_{\mathrm{DS}_{i(j+1)}}(\mathrm{EDP})\, F_{\mathrm{DS}_{i(j+1)}}(\mathrm{GP}) & \text{if } 1 \leq j < n \\ F_{\mathrm{DS}_{ij}}(\mathrm{EDP})\, F_{\mathrm{DS}_{ij}}(\mathrm{GP}) & \text{if } j = n \end{cases} \tag{7}$$

where $F_{\mathrm{DS}_{i1}}(\mathrm{EDP})$ is the fragility curve for the *j*th damage state of the *i*th structural component conditioned on the EDP=*edp* of interest; and $F_{\mathrm{DS}_{ij}}(\mathrm{GP})$ is the fragility curve that computes the probability of being or exceeding the jth damage state conditioned on the geometric parameter GP=gp of interest.

In order to estimate the probability that a building will be demolished given that it did not collapse when subjected to an earthquake with seismic intensity IM=im, the following relationship can be used,

$$P_{D|\mathrm{IM,NC}} = \int_0^\infty P_{D|\mathrm{RSDR}}\, f_{\mathrm{RSDR|IM}}\, d\mathrm{RSDR} \tag{8}$$

where $f_{\mathrm{RSDR|IM}}$ is the probability density function of the maximum residual drift ratio along the height of the building, given an intensity measure IM=im; $P_{D|\mathrm{RSDR}}$ is the probability of having to demolish the building conditioned on the maximum residual story drift ratio, RSDR, along the height of the building, which is modeled by a lognormal distribution with a median, $\mu_{D|\mathrm{RSDR}} =$ 0.015 radians and a logarithmic standard deviation, $\beta_{\ln D|\mathrm{RSDR}} = 0.3$ (Ramirez and Miranda 2012). It should be noted that these parameters are based on engineering judgment and could vary in different regions around the world. It is noted that the earthquake-induced loss computations are based on story-based EDPs as proposed by Ramirez and Miranda (2012). Based on the same methodology, in case that a residual drift concentrates in one (or few) story(ies) along the height of a building then losses because of demolition are governed by this case.

The probabilistic seismic demand model should be determined to characterize the probabilistic relationship between the EDP of interest associated with a measure of seismic demand in a frame building [e.g., peak story drift ratios (SDRs), peak absolute floor accelerations (PFAs), residual story drift ratios (RSDRs), etc.] and the seismic intensity IM=im during the earthquake event. This model is intended for the integration process over the entire range of EDPs to be used in the computations of the earthquake-induced economic losses. In this paper, the probability density functions of attaining a specified structural demand of interest given an IM=im (i.e., $f_{\mathrm{EDP|IM}}$) are assumed to follow a lognormal distribution defined by the median $\mu_{\mathrm{EDP|IM}}$ and the logarithmic standard deviation $\beta_{\mathrm{lnEDP|IM}}$ of the parameters. The parametric median $\mu_{\mathrm{EDP|IM}}$ and the associated logarithmic standard deviation $\beta_{\mathrm{lnEDP}|IM}$ are described by a power-law model form, which is fitted to the discrete data points obtained from nonlinear response history analyses [i.e., $\mu_{\mathrm{EDP|IM}} = a\,(\mathrm{IM})^b$,

$\beta_{\ln\mathrm{EDP|IM}} = c\,(\mathrm{IM})^{d}$].

An alternative earthquake-induced loss-metric that is used in this paper is the expected annual loss (EAL). The EAL is computed by numerically integrating the expected economic losses for a given seismic intensity measure IM over the entire range of a seismic hazard curve at the design site as follows,

$$\mathrm{EAL} = \int_0^{\infty} \mu_{L_{T|\mathrm{IM}}} \left| \frac{d\lambda_{\mathrm{IM}}}{d\mathrm{IM}} \right| d\mathrm{IM} \tag{9}$$

where λ_{IM} is the mean annual frequency of the seismic intensity IM at the site of interest. The advantage of using EAL is that it weights all possible levels of seismic hazard by taking into account their probability of occurrence.

DESCRIPTION OF steel-frame BUILDINGS WITH SCBFs

In order to assess the effect of gravity framing and the selected steel brace fragility curve on the loss computations of steel-frame buildings with perimeter SCBFs, four archetype office steel buildings with 2-, 3-, 6- and 12-stories are considered in this paper. The archetypes are designed as standard office buildings (i.e., occupancy category II) according to ASCE/SEI 7-05 (ASCE 2006) and ANSI/AISC 341-05 (AISC 2005). Details regarding their original design are discussed in NIST (2010). In brief, the archetypes are located on a site with stiff soil denoted as Site Class D in urban California. In order to investigate the effect of the seismic design category (SDC) on the earthquake-induced losses in steel-frame buildings with SCBFs, two sets of archetypes are selected. The first one is designed in Sacramento city (38.579°N, 121.493°W) for the lower bound of SDC D (i.e., denoted as $\mathrm{D_{min}}$). The second set of archetypes is designed in the downtown area of Los Angeles (33.996°N, 118.162°W) for the upper bound of SDC D (i.e., denoted as $\mathrm{D_{max}}$) in accordance with ASCE/SEI 7-05 (ASCE 2006).

Steel braces in the SCBFs are designed in accordance with ANSI/AISC 341-05 (AISC 2005). Round hollow structural sections (HSS) were used in most cases for the SCBF archetypes, except for the 2-story archetype SCBF building designed for SDC $\mathrm{D_{max}}$. In this case, rectangular HSS braces were used. The braces are made from ASTM A500 Grade B (i.e., nominal yield stress,

$F_{y,\text{nominal}}$=290 MPa for rectangular sections; $F_{y,\text{nominal}}$=315 MPa for round sections).

The gusset plate connections at the steel brace ends are designed in accordance with the balanced design procedure as proposed by Roeder et al. (2011) that employs an elliptical clearance distance of eight times the thickness of the gusset plate (t_p) at the corner gusset plate connections. For the design of the gusset plate connections at the mid-span of the beams, a $6t_p$ vertical clearance distance is adopted.

Figure 1 illustrates a plan view and elevation of a representative 3-story archetype building with perimeter SCBFs. The use of a 2-story X-bracing configuration is adopted [see Fig. 1(b)]. In order to investigate the effect of gravity framing on the earthquake-induced loss computations, the interior gravity framing system of each archetype building is explicitly designed in accordance with ANSI/AISC 360-10 (AISC 2010). The interior gravity columns are assumed to bend with respect to their weak axis as shown in Fig. 1(a).

Site-Specific Seismic Hazard Curves

The site-specific hazard curves for the two design locations discussed earlier are selected based on seismic hazard analysis. Figure 2(a) illustrates the design spectrum according to ASCE/SEI 7-05 (ASCE 2006). The same figure shows the design spectral acceleration, $S_a\left(T_1, 5\%\right)$ associated with the fundamental period, T_1 of the bare model representations of the archetype buildings. From this figure, it is evident that the base shear demands for SDC $\mathrm{D_{max}}$ designs are much larger than those for the SDC $\mathrm{D_{min}}$ designs.

The site-specific seismic hazard curves for all the archetype buildings are shown in Fig. 2(b). These curves are obtained from the United States Geological Survey (USGS) website. The local site condition is assumed to be the National Earthquake Hazards Reduction Program (NEHRP) site class D determined based on a shear wave velocity v_s of $259 m/s$. To better facilitate the EAL as well as the mean annual frequency of collapse, λ_c computations, a fourth-order polynomial is fitted to the selected hazard curves (Eads et al. 2013).

Assumed Fragility Curves and Cost Distribution Functions

In order to reliably estimate the earthquake-induced losses in the archetype buildings their architectural layout is developed by assuming a rectangular floor area of $2007m^2$ ($21,600ft^2$). The replacement cost for an archetype building is assumed to be \$1880 (based on 2013 U.S. dollars) per square meter (i.e., \$175 per square foot). This estimation is based on the RS Means Square Foot Costs (RS Means 2013) for urban California. This is a rational cost estimate based on prior building-specific loss estimation studies (Dyanati et al. 2015).

In order to reliably quantify the earthquake-induced losses for the archetype buildings discussed herein in a probabilistic manner, it is essential to carefully define the fragility curves of their structural and nonstructural components. In an effort to retain simplicity in the loss computations, current probabilistic building-specific loss estimation methodologies (FEMA 2012) utilize univariate fragility curves (e.g., drift- or acceleration-based). However, damageable components may be very sensitive to other geometric and/or material parameters that we tend to ignore (Aslani and Miranda 2005; Lignos and Karamanci 2013). In order to quantify the effect of the used fragility curves on earthquake-induced economic losses of the archetypes discussed earlier, we utilize drift-based and dual-parameter fragility curves for steel braces as discussed in Lignos and Karamanci (2013). An example of such curves is shown in Fig. 3 for global buckling of round HSS braces. Referring to Fig. 3(a), the probability of occurrence of flexural buckling in round HSS braces at 0.5% SDR is 50%. However, depending on the global slenderness, KL/r of the respective brace (where K is the effective length factor, L is the length of the brace, and r is the radius of gyration) this value can be much larger or much smaller for the same SDR as shown in Fig. 3(b). Table 1 lists the dual-parameter fragility curves for all the considered damage states of round HSS braces.

Table 2 summarizes the repair cost associated with damage states for each damageable component identified in the archetype buildings including the respective fragility distribution curve documented in prior studies (FEMA 2012; Ramirez et al. 2012; Lignos and Karamanci 2013). The fragility parameters in Table 2 for steel columns and column splices refer to the steel-frame building performance (i.e., story-based EDP fragility curves). However, losses because of repair actions in such structural components are only considered if the corresponding component undergoes inelastic deformation. The fragility curves used in this paper are primarily adopted by FEMA P-58 and other recently published literature (see Table 2). According to FEMA P-58 background documentation [see Section 1 in Deierlein and Victorsson (2008)], in modern capacity-designed steel-frame buildings it can be assumed that the framing elements (beams and columns) and their connections, as well as the brace-to-frame connections are strong enough such that the inelastic action will primarily occur in the braces through cyclic tension and compression as well as the column bases (FEMA 2012). For this reason, fragility curves that describe the various damage states and the associated repair costs for beam-to-column panel zone joints are not currently available in FEMA P-58 (FEMA 2012).

NONLINEAR BUILDING MODELS AND SIMULATION OF STRUCTURAL COLLAPSE

The analytical model representation of the archetype buildings is developed within the Open System for Earthquake Engineering Simulation Platform (OPENSEES) (McKenna 1997). In order to evaluate the effect of gravity framing system on the earthquake-induced economic losses, two analytical model representations of the archetype buildings are developed. The first one considers the bare steel SCBF (i.e., bare SCBFs model, subsequently referred to as B model); the second model explicitly considers the composite floor action and the interior gravity framing system (i.e., subsequently referred to as CG model) as discussed in Elkady and Lignos (2015).

The lateral load-resisting system of each building located in the east-west (E-W) loading direction [see Fig. 1(a)] is modeled in 2-dimensions (2-D). For illustration purposes, Fig. 4 shows the analytical model representation of a 3-story SCBF. In brief, all steel beams and columns are modeled as elastic elements with concentrated plasticity springs at their ends based on the modified Ibarra-Medina-Krawinkler (IMK) deterioration model (Ibarra et al. 2005; Lignos and Krawinkler 2011). The panel zone shear distortion is explicitly modeled as discussed in Gupta and Krawinkler (1999). The steel braces in the SCBFs consist of 8 displacement-based fiber elements that are able to trace flexural buckling as well as fracture initiation because of low-cycle fatigue based on the modeling recommendations developed by Karamanci and Lignos (2014). Figure 4(c) illustrates a comparison of the measured and simulated hysteretic axial force-axial displacement relation of a rectangular HSS steel brace based on the modeling recommendations discussed in Karamanci and Lignos (2014). In this figure, the experimental data were retrieved from Han et al. (2007). A non-linear out-of-plane rotational spring [see Figs. 4(a) and (b)] is placed at the ends of each brace to explicitly simulate the flexibility and flexural yielding of the gusset plates because of out-of-plane brace bending as proposed by Hsiao et al. (2013).

Second order effects (i.e., P-Delta effects) are explicitly considered in both B and CG models by connecting a '*leaning column*' and an '*equivalent gravity frame*', respectively, with a steel SCBF through axially rigid links. The corotational transformation is used in OpenSees to consider the second order effects.

For CG models the effect of composite action on the interior gravity framing system is explicitly captured in the CG models as discussed in Elkady and Lignos (2015). This necessitates a realistic representation of typical shear tab beam-to-column connections used in steel-frame buildings in North America in accordance with ANSI/AISC 360-10 (AISC 2010). The shear tab beam-to-column connections that are considered in this paper consist of a single steel plate fillet welded to the supporting column with a single column of structural bolts. The distance between the beam flange to the column face is 25*mm*. Experimental research of similar composite shear tab beam-to-column connections (Liu and Astaneh-Asl 2000) suggests that such connections can sustain up to about 40% of the fixed end moment of the steel beam with an appreciable plastic deformation capacity. Figure 4(d) illustrates a comparison of the measured and simulated moment-rotation hysteretic relation of a composite beam as part of a single-plate shear tab beam-to-column connection. From this figure, the modeling approach used for composite shear tab beam-to-column connections reflects the experimental results.

Structural Collapse Simulations and Associated Collapse Risk

To determine the probabilistic relationship between EDPs and IM, the analytical model representations of the archetype buildings discussed earlier are subjected to a set of 44 Far-Field ground motions obtained from FEMA P695 (FEMA 2009). This set of ground motions includes twentytwo component pairs of horizontal ground motion records from sites located in a distance greater than or equal to 10 *km* from the fault rupture. The magnitude M_w range of the ground motion set is from M_w 6.5 to 7.6. These ground motions represent well the seismic hazard of urban California and in particular the design location of the archetype buildings. More details regarding the selected ground motion set can be found in FEMA P695 (FEMA 2009).

Incremental dynamic analysis (IDA) (Vamvatsikos and Cornell 2002) is used in order to trace the dynamic collapse because of sidesway instability for each archetype building. The critical EDPs of interest (i.e., peak SDRs, PFAs and RSDRs) are monitored for each ground motion over the full range of seismic intensities until the occurrence of structural collapse. Based on these recorded EDPs, the probabilistic relationship of multiple EDPs and IM is established. In this case, the $S_a(T_1, 5\%)$ is used as an IM. However, other IMs could be used in this process as discussed in recent studies (Eads et al. 2015; Kazantzi and Vamvatsikos 2015; Kohrangi et al. 2016). Figures 5(a) and (b) illustrate the IDA curves in terms of IM [i.e., the 5% damped spectral acceleration at the first mode of the building $S_a(T_1, 5\%)$] versus the maximum SDRs obtained from the CG model of the 3- and 12-story steel-frame buildings with SCBFs, respectively. In these figures, the additional vertical axis at the right of each figure represents the normalized spectral acceleration with respect to the 5% damped design-basis spectral acceleration of each steel-frame building. The counted median, 16^{th} and 84^{th} percentiles determined based on the suite of 44 ground motions are also superimposed in Fig. 5.

Results from nonlinear response history analysis indicate that most of the gravity columns in the archetypes remained elastic before losses because of collapse and building demolition start to govern the total losses (i.e., up to MCE seismic intensity). For example, in the case of the 12-story CG model designed for SDC D_{max}, its gravity columns only in the upper two stories experienced inelastic deformation up to about 4% (i.e., 0.6% inelastic deformation on average) for 24 out of 32 non-collapsing ground motions scaled at the MCE seismic intensity.

The resulting collapse capacities and record-to-record variability for each archetype are adjusted to take into account the spectral shape effects as discussed in Haselton et al. (2011). Figure

6 illustrates the adjusted collapse fragility curves as computed based on the B and CG models for the SDC D_{max} and D_{min}. These curves describe the probability of collapse $P_{C|IM}$ as a function of the spectral acceleration at the first mode period of the respective archetype of interest, $S_a(T_1, 5\%)$. From this figure, it is evident that when the composite slab action and the interior gravity framing system are considered as part of the analytical model representation, the collapse capacity of a building is normally increased, compared to that computed based on a B model regardless of the seismic design category.

Table 3 summarizes the median collapse capacities, $\hat{S}_{CT}\,(T_1, 5\%)$ and logarithmic standard deviations, β_{RTR} of the aforementioned collapse fragility curves for all the analytical model representations of the archetype buildings under consideration. From this table, the composite floor system and the gravity framing typically increase the collapse capacity by 26% and 40% on average, for SDC D_{max} and D_{min}, respectively, compared to the collapse capacities computed based on the B model building representations.

The reason why the adjusted median collapse capacity and standard deviation of the 3-story archetype is nearly the same regardless of the used nonlinear building model is that the main collapse mechanisms observed based on the B and CG models are practically the same for the given set of ground motions. Figure 7 shows the main collapse mechanisms including the number of collapses per mechanism out of the 44 ground motions observed in the 3-and 6-story SCBFs based on the B and CG models. The latter is indicated as a fraction above each collapse mechanism shown in Figure 7. Referring to Figures 7(a) and 7(b), it is evident that when the gravity framing is included in the analytical model representation of the 3-story archetype there is practically no change in the number of possible collapse mechanisms. The number of collapses per mechanism is nearly identical in both cases excluding 2 ground motions in which the collapse mechanism shifted from mode III to mode II when the gravity framing was included in the nonlinear building model representation [see Figs. 7(a) and 7(b)]. In this case, the standard deviation of the collapse capacity of the 3-story archetype increases when the CG model is used compared to that computed based on the B model. Referring to Figures 7(a) and 7(b), although the total number of possible collapse mechanisms of the 3-story SCBF did not change when a CG model was utilized the number of collapse mechanisms, which require fewer bracing members to fracture, was reduced.

Similarly, Figures 7(c) and 7(d) illustrate the possible collapse mechanisms for the 6-story archetype when the B and CG models are used, respectively. From these figures, when the gravity framing is included in the nonlinear building model, the number of possible collapse mechanisms drops from 7 to 4 in this case. From the resultant collapse mechanisms [see Figure 7(d)] it is evident that the gravity framing better distributes the peak SDRs along the height of a SCBF and prevents the concentration of inelastic deformations into single stories. In this case, the median collapse capacity of the archetype increases considerably. Furthermore, the corresponding standard deviation of the collapse fragility curve of the 6-story SCBF based on the CG model becomes smaller compared to that obtained from the B model because the total number of the collapse mechanisms becomes less [see Figures 7(c) and 7(d)].

Figure 8 illustrates the mean annual frequency of collapse λ_c of the analytical model representation of the archetype buildings designed for SDC D_{max} [see Fig. 8(a)] and D_{min} [see Fig. 8(b)]. The additional vertical axes at the right of each figure corresponds to a probability of collapse over a 50-year return period, $P_c\,(\text{in 50 years})$ by assuming a Poisson distribution. From these figures, it is evident that the estimated collapse risk of archetype buildings with SCBFs designed for SDC D_{max} and D_{min} can be reduced by a factor of 2, on average, when incorporating the composite slab action and the gravity framing system into the analytical model representation of the respective building of interest. In this case, the 1% over 50 years collapse risk limit adopted in ASCE/SEI 7-10 (ASCE 2010) is also respected regardless of the number of stories of the respective archetype steel-frame building. In most cases, such limit is not respected otherwise if a B model representation is used. Therefore, the collapse risk of steel-frame buildings with SCBFs can be severally overestimated in highly seismic regions if a B model is used.

EXPECTED LOSSES CONDITIONED ON SEISMIC INTENSITY

Figure 9 shows the normalized loss vulnerability curves for the 3- and 12-story archetype buildings designed for a SDC D_{max} and D_{min} based on the B model representations. In this figure, loss computations are based on univariate (i.e., drift- or acceleration-based) fragility curves for each damageable component according to Table 2. Referring to Fig. 9, the expected losses (i.e., vertical axis) are normalized with respect to the corresponding building total replacement cost that is summarized in Table 4. The vulnerability curves illustrate the expected economic losses in an archetype building as a function of the IM, $S_a(T_1, 5\%)$. In Fig. 9, the expected losses conditioned on a seismic intensity are further disaggregated into losses because of structural and nonstructural component repairs, losses because of demolition given that building collapse did not occur and losses because of dynamic collapse. In order to put the expected losses into perspective, the horizontal axes at the top of Fig. 9 illustrate the IM normalized with respect to the spectral acceleration corresponding to a design-basis earthquake (DBE) [i.e., $S_a(T_1, 5\%)$@DBE] as specified in ASCE/SEI 7-05 (ASCE 2006). These values can be obtained directly from Fig. 2(a) if the predominant period of the respective archetype building is known.

Referring to Fig. 9, the primary contributor to the expected losses is that from nonstructural component repairs up to the DBE seismic intensity regardless of the number of stories of the respective archetype building and the seismic design category. For the 12-story archetype building designed with SDC D_{max} [see Fig. 9(b)], losses are governed by building demolition because of excessive residual deformations along its height as well as losses because of structural collapse at 1.5×DBE seismic intensities [i.e., a maximum considered earthquake (MCE)]. In that respect, this is important particularly for mid- and high-rise steel-frame buildings designed in highly seismic regions, which are vulnerable to P-Delta effects and therefore, residual deformations may become a controlling issue. This agrees with recent research on steel special moment frames (Hwang et al. 2015; Hwang and Lignos 2017). For archetype buildings designed with SDC D_{min} [see Figs. 9(c) and (d)], losses because of building demolition and structural collapse are insignificant at the MCE seismic intensity, regardless of the number of stories of the archetype building. This is in agreement with the collapse risk of the same buildings as shown in Fig. 8. The aforementioned observations are further elaborated in the subsequent paragraphs.

Figures 10 and 11 show the expected losses based on B and CG model representations of selected archetype buildings at two seismic intensities of interest (i.e., DBE and MCE) at the design site of interest for SDC D_{max} and D_{min}, respectively. In the same figures, the influence of the used steel brace fragility curve (i.e., univariate versus bivariate) to the expected losses is also examined. Referring to Figs. 10 and 11, at moderate seismic intensities (i.e., DBE seismic intensity), losses because of nonstructural component repairs seem to be indifferent to the respective analytical model representation. In particular, losses because of the acceleration-sensitive nonstructural component repairs become a major contributor to the expected total losses regardless of the number of stories. It is worth mentioning that the contribution of structural repairs to the total losses at the DBE seismic intensity is appreciable in most cases. This is attributed to flexural buckling of the round HSS braces. This typically occurs at SDRs in the range of 0.5%, on average (Roeder et al. 2012; Lignos and Karamanci 2013). However, when the effect of steel brace global slenderness or local slenderness on the corresponding fragility curve is explicitly captured, the computed losses because of steel brace flexural buckling are reduced by 20%, on average, with respect to those computed based on drift-based steel brace fragility curves. This observation holds true regardless of the used seismic design category (see Figs. 10 and 11).

Referring to Fig. 10, at seismic intensities associated with low probability of occurrence earthquakes (i.e., MCE hazard level) in highly seismic regions (i.e., SDC D_{max}), economic losses for mid- and high-rise steel-frame buildings are largely governed by building demolition when EDPs are based on the bare steel SCBF (i.e., B model). This is attributed to the excessive predicted residual deformations along the building height. This observation holds true regardless of the used steel brace fragility curve. It is noteworthy that when the gravity framing is explicitly considered as part of the analytical model representation of the same archetype buildings, losses because of demolition at the MCE intensity are reduced by 27 to 92% compared to those predicted from the B models. This indicates the importance of the gravity framing system in the reduction of the destabilizing (P-Delta) influence of the gravity load on steel-frame buildings with SCBFs.

Referring to Figs. 10(b) and (c), in mid- and high-rise archetype buildings designed with SDC D_{max}, losses because of structural collapse based on CG models are decreased significantly than those computed based on B models. This observation is attributed to the fact that the drift concentration is not limited only to a few stories of a steel-frame building with SCBFs when the interior gravity framing system is included into the analytical model (Ji et al. 2009). Therefore, more stories (i.e., more steel braces) participate into the energy dissipation during an earthquake. This also agrees well with findings from earlier studies on the contribution of the gravity framing system to the reserve capacity of steel braced frame buildings without any special detailing requirements for seismic loading (Stoakes and Fahnestock 2011; Fahnestock et al. 2014).

It is noteworthy that losses because of building demolition do not become a controlling issue for archetypes in relatively moderate seismicity zones (i.e., SDC D_{min}) (see Fig. 11). This holds true even for taller buildings that may be sensitive to P-Delta effects. In such cases, B model building representations may be used for building-specific loss assessment. This is because of the fact that very few braces fracture along the height of archetypes designed for SDC D_{min} at the MCE intensity. For instance, looking at the simulation results from 30 out of 44 ground motions scaled at the MCE intensity that structural collapse did not occur in the CG model representation of the 12-story D_{min} archetype, only 3 braces fractured over the frame height during 9 out of 30 ground motions. In contrast, at the MCE intensity, the CG model building representation of the 12-story D_{max} archetype experienced many more brace fractures. In addition, some of its stories lost completely both braces. Therefore, plastic deformations concentrated in these stories and structural collapse occurred because of P-Delta effects.

EXPECTED ANNUAL LOSSES

In this section, the earthquake-induced losses in steel-frame buildings with SCBFs are evaluated based on the EAL. This loss-metric is computed by integrating the site-specific seismic hazard curves shown in Fig. 2(b) over the corresponding vulnerability curves shown in Fig. 9. The advantage of using EAL as a loss-metric compared to the loss vulnerability curves discussed earlier is that EAL is calculated by considering all possible levels of seismic hazard at the design site and their probability of occurrence. Therefore, the contribution of frequent seismic events on building-specific loss estimation is more pronounced compared to loss computations at a given seismic intensity.

Figure 12 illustrates the EALs for the 3- and 12-story archetype buildings designed for SDC D_{max} and D_{min}. Additionally, the corresponding present value (*P.V.*) of life-cycle costs is provided in the vertical axis at the right side of each figure. The *P.V.* is simply computed by multiplying a building's EAL times its expected remaining life, T with a discount rate, $r = 3\%$ $\left[= EAL \times \sum_{i=1}^{T} (1+r)^{-i}\right]$. In this paper, the expected remaining life of a building is assumed to be 50 years (i.e., office building). Referring to Fig. 12, EALs and *P.V.* are normalized with respect to the total replacement cost of the respective building. For comparison purposes, both the B and CG model representations of the 3- and 12-story archetypes are facilitated to compute the EALs as well as the *P.V.* In order to capture the sensitivity of the EAL on the used steel brace fragility curve, the EALs are computed based on drift-based and dual-parameter steel brace fragility curves (Lignos and Karamanci 2013). In Fig. 12, EALs are further disaggregated into losses because of repairs of structural and nonstructural building components (i.e., drift-sensitive and acceleration-sensitive), building demolition as well as collapse losses.

From Fig. 12, the EALs are practically not sensitive to the choice of the used analytical model representation nor the used steel brace fragility curve. Therefore, the simplest possible combination can be utilized for building-specific loss assessment when the EAL is used as a loss-metric. Same observations hold true for the rest of the archetypes that were evaluated based on their EALs that are summarized in Table 4. From this table, the normalized EALs for archetype buildings with SCBFs typically range from 0.74 to 0.87% for SDC D_{max} and from 0.39 to 0.65% for SDC D_{min}. These values are consistent but slightly larger than the EALs computed for other frame buildings with conventional steel and reinforced concrete lateral load-resisting systems in North America (Ramirez et al. 2012; Hwang et al. 2015; Hwang and Lignos 2017).

Figure 12 illustrates that losses because of repairs in acceleration-sensitive nonstructural components dominate the total EALs regardless of the analytical model representation (i.e., B or CG model), the selected steel brace fragility curve and the used seismic design category. steel-frame buildings that utilize SCBFs are inherently stiff; therefore, absolute floor acceleration demands along their height are expected to be larger than those in moment-resisting frame systems. On the other hand, losses because of repairs in drift-sensitive nonstructural components seem to be negligible in all cases because of the added lateral stiffness that steel braces provide compared to steel moment-resisting frame systems. Referring to Fig. 12, the contribution of SCBF structural repairs to the EALs can be appreciable for mid- and high-rise archetypes. This is attributed to flexural buckling of steel braces at fairly small SDRs (i.e., 0.5%) that can be associated to frequent and moderately frequent seismic events (i.e., 50% and 10% probability of occurrence over 50 years).

From Table 4 and Fig. 12, the contribution of demolition and collapse losses to the EALs is not significant. Such contributions are expected to dominate losses at seismic intensities with low probability of occurrence (i.e., extreme events). However, these events have a small weight on the EAL computations compared to that of frequent seismic events (i.e., mean annual frequency λ_{IM} of occurrence are 2.1×10^{-3} and 4.0×10^{-4} at given hazard levels of DBE and MCE, respectively). If the emphasis of building-specific loss estimation as well as building performance is at large deformations associated with structural collapse then it is recommended that losses conditioned on the seismic intensity of interest should be used as a loss-metric. In this case, the nonlinear building model representation should explicitly consider the gravity framing system and the composite floor action.

LIMITATIONS

This paper summarizes a comprehensive investigation on the effects of modeling choices as well as the used component fragility curves on the collapse risk and probabilistic economic loss assessment of steel-frame buildings with SCBFs. However, a number of limitations of the present study should be pointed out. Such limitations may provide the basis for further research. In particular:

- Even though the rotational stiffness of the column base connection may significantly affect the structural response [see Zareian and Kanvinde (2013)], the column bases are idealized as *fixed*. Experimental studies on steel column base connections [e.g., Kanvinde et al. (2012) and Borzouie et al. (2014)] as well as reconnaissance reports on steel-frame buildings (Clifton et al. 2011; MacRae et al. 2015) suggest that a lower rotational stiffness should be used than that used in practice for "*fixed*" column base connections [e.g., fixed base value of $1.67(EI/L)_{\text{column}}$ specified in current New Zealand provisions (NZS 2007)]. Despite that primary structural elements in the capacity-designed superstructure may be undergoing considerable yielding, the inherent column base flexibility may significantly reduce the expected plastic deformation at the column base that ultimately affects the residual drift in the bottom story of a frame building. This issue deserves more attention and should be investigated in future studies.

- The response of steel-frame buildings to earthquake shaking affected by the soil-foundation-structure interaction (SFSI) is not considered in this paper. This may be a critical consideration in cases that structural damage was not observed in steel-frame buildings (MacRae et al. 2015), This is consistent with prior analytical studies on the beneficial effect of SFSI on structural performance (i.e., reduction in peak SDRs, PFAs as well as residual deformations) in multi-story buildings (Givens et al. 2012; NIST 2012a; Storie et al. 2014). Therefore, the probabilistic economic losses may be overstated when ignoring the SFSI effect into the analytical model representation of the respective building. This issue deserves more attention in future research studies.
- Losses because of repair or replacement of acceleration-sensitive nonstructural components herein are derived based on fragility curves with fairly low median PFAs at each damage state as suggested in FEMA P-58 (FEMA 2012). However, this may not be consistent with damage observations in steel-frame buildings from the 2010/2011 Christchurch earthquakes (Clifton et al. 2011). In particular, no damage was observed to either the suspended ceilings or the sprinkler (i.e., components sensitive to PFAs) installed in steel buildings subjected to a PGA of 0.55 g and PFAs of 0.55–0.7 g. Therefore, loss estimation of nonstructural acceleration-sensitive components may be conservative to some extent.
- The earthquake-induced economic losses presented herein are based on fragility curves for

building components available in recently published literature (FEMA 2012; Ramirez et al. 2012; Lignos and Karamanci 2013). For instance, specific components such as elevator repairs may be more influenced by residual drifts instead of PGA, as the lift shaft guiderails may require realignment in the case of permanent deformations along the height of a building (Clifton et al. 2011). Therefore refined component fragility curves should be developed when new experimental data become available.

CONCLUSIONS

This paper assessed the effect of analytical modeling assumptions on the collapse risk and the earthquake-induced economic losses for typical archetype steel-frame buildings with special concentrically braced frames (SCBFs) ranging from 2- to 12-stories. This was achieved through the development of analytical model representations of the bare SCBF only (namely as B model) as well as models that captured explicitly the effect of the gravity framing and the composite floor action (namely as CG model) on the steel-frame building's structural response. Typical archetypes were designed in two different seismic zones in urban California; the first one represented the lower bound of the Seismic Design Category D (referred to as SDC D_{min}); and the second one represented the upper bound of the Seismic Design Category D (referred to as SDC D_{max}). A comprehensive probabilistic loss estimation methodology was used (Ramirez and Miranda 2012) and refined that rigorously integrates multiple engineering demand parameters (EDPs) for a wide range of seismic intensities representing frequent seismic events as well as earthquakes with low probability of occurrence. The earthquake-induced economic losses were evaluated in terms of expected losses conditioned on a seismic intensity (i.e., loss vulnerability curves) and the expected annual losses (EALs). The effect of the used steel brace fragility curve on the loss computations was also quantified. The main findings are summarized as follows:

1. Damage in acceleration-sensitive nonstructural components seem to govern the total losses in steel-frame buildings with SCBFs at frequent and design basis seismic events. The magnitude of such losses is not sensitive to the selected analytical model representation,

the number of stories of the respective archetype building and the used loss-metric.

2. Losses because of steel brace damage seem to be appreciable at frequent and design-basis earthquakes. This is because of the fact that steel brace flexural buckling may occur at fairly small drift ratios (i.e., 0.5% on average). In this case, the choice of the used steel brace fragility curve affects the loss computations. In particular, drift-based fragility curves commonly used in the earthquake engineering practice tend to overestimate repairs of steel brace components by approximately 20% compared to dual-parameter steel brace fragility curves. The latter captures the effect of brace geometry (i.e., global and local slenderness) on loss computations for a given story drift ratio.
3. If losses because of demolition and collapse are of fundamental concern, they should be evaluated conditioned on the seismic intensity of interest. In this case, the choice of the analytical model representation of the archetype building becomes significant especially for steel-frame buildings designed in highly seismic regions (i.e., SDC D_{max}). In particular, nonlinear building models that explicitly capture the destabilizing effects of the gravity framing (i.e., CG models) should be used. Else, losses because of demolition are largely overestimated because of drift concentrations in few stories of a steel SCBF that in reality are not as pronounced as B models predict.
4. steel-frame buildings with perimeter SCBFs designed for a SDC D_{max} achieved a probability of collapse in 50 years that satisfied the 1% limit specified by ASCE/SEI 7-10 (ASCE 2010) only when the contribution of the composite slab action and the gravity framing was considered as part of the analytical model building representation. Models that consider the bare frame only seem to largely overestimate the collapse risk of steel-frame buildings with SCBFs in highly seismic regions. This is not a controlling issue for steel SCBFs designed for a SDC D_{min}.
5. The EAL is a more representative metric to evaluate losses in steel-frame buildings with SCBFs for seismic events with moderate to high probability of occurrence (i.e., more frequently occurring seismic events) compared to loss-metrics that are conditioned on a single

seismic intensity. The reason is that more frequent seismic events are better weighted in the EAL computations through the integration of the loss vulnerability curve of a building over the design site-specific hazard curve. In this case, detailed modeling of the respective building of interest does not seem to be critical for the cases considered in this paper.

6. The normalized EALs for low- to high-rise steel-frame buildings with SCBFs range from 0.74 to 0.87% for SDC D_{max} and from 0.39 to 0.65% for SDC D_{min}. These values seem to be insensitive to the choice of the analytical modeling representation of the respective archetype and the choice of the steel brace fragility curve. In addition, the above EAL range is consistent but slightly larger than the corresponding values for other conventional steel and reinforced concrete frame buildings designed in seismic regions.

ACKNOWLEDGMENTS

This study is based on work supported by the Fonds de recherché du Québec - Nature et technologies, Projet de Recherché en Equipe, Award No. FQRNT 2013-PR-167747. Financial support was also provided by the Swiss Federal Institute of Technology in Lausanne (EPFL). The financial support is gratefully acknowledged. Any opinions, findings, and conclusions or recommendations expressed in this paper are those of the authors and do not necessarily reflect the views of the sponsors.

REFERENCES

AISC (2005). "Seismic provisions for structural steel buildings." *ANSI/AISC 341-05*, American Institute of Steel Construction, Chicago, IL.

AISC (2010). "Specification for structural steel buildings." *ANSI/AISC 360-10*, American Institute of Steel Construction, Chicago, IL.

Aitchison, J. and Brown, J. A. C. (1957). *The lognormal distribution with special reference to its uses in Economics*. Cambridge University Press, Cambridge.

ASCE (2006). "Minimum design loads for buildings and other structures." *ASCE/SEI 7-05*, American Society of Civil Engineers, Reston, VA.

ASCE (2010). "Minimum design loads for buildings and other structures." *ASCE/SEI 7-10*, American Society of Civil Engineers, Reston, VA.

Aslani, H. and Miranda, E. (2005). "Fragility assessment of slab-column connections in existing non-ductile reinforced concrete buildings." *Journal of Earthquake Engineering*, 9(6), 777–804.

Baradaran Shoraka, M., Yang, T. Y., and Elwood, K. J. (2013). "Seismic loss estimation of non-ductile reinforced concrete buildings." *Earthquake Engineering & Structural Dynamics*, 42(2), 297–310.

Borzouie, J., MacRae, G. A., Chase, J. G., and Clifton, G. C. (2014). "Experimental studies on cyclic behaviour of steel base plate connections considering anchor bolts post tensioning." *Proceedings of 2014 New Zealand Society for Earthquake Engineering Annual Conference*, Auckland, New Zealand.

Chopra, A. K. (2011). *Dynamics of structures: Theory and applications to earthquake engineering*. Prentice Hall, Upper Saddle River, NJ, 4th edition.

Clifton, G. C., Bruneau, M., MacRae, G., Leon, R., and Fussell, A. (2011). "Steel structures damage from the Christchurch earthquake series of 2010 and 2011." *Bulletin of the New Zealand Society for Earthquake Engineering*, 44(4), 297–318.

Cornell, C. A. and Krawinkler, H. (2000). "Progress and challenges in seismic performance assessment." *PEER Center News*, 3(2), 1–3.

Deierlein, G. G. and Victorsson, V. (2008). "Fragility curves for components of steel SMF systems." *Background document of FEMA P-58/BD-3.8.3*, prepared by the Applied Technology Council for the Federal Emergency Management Agency, Washington, DC.

Dyanati, M., Huang, Q., and Roke, D. (2015). "Life cycle cost-benefit evaluation of self-centering and conventional concentrically braced frames." *Proceedings of 12th International Conference on Applications of Statistics and Probability in Civil Engineering, ICASP12*, Vancouver, BC, Canada.

Eads, L., Miranda, E., Krawinkler, H., and Lignos, D. G. (2013). "An efficient method for estimating the collapse risk of structures in seismic regions." *Earthquake Engineering & Structural Dynamics*, 42(1), 25–41.

Eads, L., Miranda, E., and Lignos, D. G. (2015). "Average spectral acceleration as an intensity measure for collapse risk assessment." *Earthquake Engineering & Structural Dynamics*, 44(12), 2057–2073.

Elkady, A. and Lignos, D. G. (2015). "Effect of gravity framing on the overstrength and collapse capacity of steel frame buildings with perimeter special moment frames." *Earthquake Engineering & Structural Dynamics*, 44(8), 1289–1307.

Fahnestock, L. A., Hines, E. M., Tremblay, R., Bradley, C., Nelson, J., Beland, T., Davaran, A., and Sizemore, J. (2014). "Reserve capacity and implications for seismic collapse prevention for low-ductility braced frames in moderate seismic regions." *Proceedings of 10th U.S. National Conference on Earthquake Engineering: Frontiers of Earthquake Engineering*, Anchorage, AK.

FEMA (2009). "Quantification of building seismic performance factors." *Report No. FEMA-P695*, Federal Emergency Management Agency, Washington, DC.

FEMA (2012). "Seismic performance assessment of buildings, volume 1-methodology." *Report No. FEMA P-58-1*, prepared by the Applied Technology Council for the Federal Emergency Management Agency, Washington, DC.

Flores, F. X., Charney, F. A., and Lopez-Garcia, D. (2014). "Influence of the gravity framing system on the collapse performance of special steel moment frames." *Journal of Constructional*

Steel Research, 101, 351–362.

Flores, F. X., Charney, F. A., and Lopez-Garcia, D. (2016). "The influence of gravity column continuity on the seismic performance of special steel moment frame structures." *Journal of Constructional Steel Research*, 118, 217–230.

Givens, M. J., Stewart, J. P., Haselton, C. B., and Mazzoni, S. (2012). "Assessment of soil-structure interaction modeling strategies for response history analysis of buildings." *Proceedings of the 15th World Conference on Earthquake Engineering (15WCEE)*, Lisbon, Portugal.

Gupta, A. and Krawinkler, H. (1999). "Seismic demands for the performance evaluation of steel moment resisting frame structures." *Blume Center Technical Report No. 132*, The John A. Blume Earthquake Engineering Center, Stanford University, Stanford, CA.

Han, S.-W., Kim, W. T., and Foutch, D. A. (2007). "Seismic behavior of HSS bracing members according to width-thickness ratio under symmetric cyclic loading." *Journal of Structural Engineering*, 133(2), 264–273.

Haselton, C. B., Baker, J. W., Liel, A. B., and Deierlein, G. G. (2011). "Accounting for ground-motion spectral shape characteristics in structural collapse assessment through an adjustment for epsilon." *Journal of Structural Engineering*, 137(3), 332–344.

Hsiao, P.-C., Lehman, D. E., and Roeder, C. W. (2013). "A model to simulate special concentrically braced frames beyond brace fracture." *Earthquake Engineering & Structural Dynamics*, 42(2), 183–200.

Hwang, S.-H., Elkady, A., Bardaweel, S. A., and Lignos, D. G. (2015). "Earhtuqake loss assessment of steel frame buildings desinged in highly seismic regions." *Proceedings of 5th ECCOMAS Thematic Conference on Computational Methods in Structural Dynamics and Earthquake Engineering*, Crete Island, Greece, 1496–1512.

Hwang, S.-H. and Lignos, D. G. (2017). "Earthquake-induced loss assessment of steel frame buildings with special moment frames designed in highly seismic regions." *Earthquake Engineering & Structural Dynamics* , DOI:10.1002/eqe.2898, in press.

Ibarra, L. F., Medina, R. A., and Krawinkler, H. (2005). "Hysteretic models that incorporate strength and stiffness deterioration." *Earthquake Engineering & Structural Dynamics*, 34(12), 1489–1511.

Ji, X., Kato, M., Wang, T., Hitaka, T., and Nakashima, M. (2009). "Effect of gravity columns on mitigation of drift concentration for braced frames." *Journal of Constructional Steel Research*, 65(12), 2148–2156.

Kanvinde, A. M., Grilli, D. A., and Zareian, F. (2012). "Rotational stiffness of exposed column base connections: Experiments and analytical models." *Journal of Structural Engineering*, 138(5), 549–560.

Karamanci, E. and Lignos, D. G. (2014). "Computational approach for collapse assessment of concentrically braced frames in seismic regions." *Journal of Structural Engineering*, 140(8), A4014019.

Kazantzi, A. K. and Vamvatsikos, D. (2015). "Intensity measure selection for vulnerability studies of building classes." *Earthquake Engineering & Structural Dynamics*, 44(15), 2677–2694.

Kohrangi, M., Bazzurro, P., and Vamvatsikos, D. (2016). "Vector and scalar IMs in structural response estimation, part II: Building demand assessment." *Earthquake Spectra*, 32(3), 1525–1543.

Li, Y. and van de Lindt, J. W. (2012). "Loss-based formulation for multiple hazards with application to residential buildings." *Engineering Structures*, 38, 123–133.

Liel, A. B. and Deierlein, G. G. (2013). "Cost-benefit evaluation of seismic risk mitigation alternatives for older concrete frame buildings." *Earthquake Spectra*, 29(4), 1391–1411.

Lignos, D. G. and Karamanci, E. (2013). "Drift-based and dual-parameter fragility curves for concentrically braced frames in seismic regions." *Journal of Constructional Steel Research*, 90, 209–220.

Lignos, D. G. and Krawinkler, H. (2011). "Deterioration modeling of steel components in support of collapse prediction of steel moment frames under earthquake loading." *Journal of Structural Engineering*, 137(11), 1291–1302.

Liu, J. and Astaneh-Asl, A. (2000). "Cyclic testing of simple connections including effects of slab."

Journal of Structural Engineering, 126(1), 32–39.

MacRae, G., Clifton, G. C., Bruneau, M., Kanvinde, A., and Gardiner, S. (2015). "Lessons from steel structures in Christchurch earthquakes." *Proceedings of 8th International Conference on Behavior of Steel Structures in Seismic Areas (STESSA)*, Shanghai, China, 1474–1481.

MacRae, G. A., Kimura, Y., and Roeder, C. (2004). "Effect of column stiffness on braced frame seismic behavior." *Journal of Structural Engineering*, 130(3), 381–391.

MATLAB Version 8.5.0 (R2015a) (2015). The Math Works, Inc., Natick, MA.

McKenna, F. T. (1997). "Object oriented finite element programming frameworks for analysis, algorithms and parallel computings." Ph.D. thesis, University of California at Berkeley, Berkeley, CA.

Mitrani-Reiser, J. (2007). "An ounce of prevention: probabilistic loss estimation for performance-based earthquake engineering." Ph.D. thesis, California Institute of Technology, Pasadena, CA.

NIST (2010). "Evaluation of the FEMA P-695 methodology for quantification of building seismic performance factors." *Report No. NIST GCR 10-917-8*, prepared by the NEHRP Consultants Joint Venture for the National Institute of Standards and Technology, Gaithersburg, MD.

NIST (2012a). "Soil-structure interaction for building structures." *Report No. NIST GCR 12-917-21*, prepared by the NEHRP Consultants Joint Venture for the National Institute of Standards and Technology, Gaithersburg, MD.

NIST (2012b). "Tentative framework for development of advanced seismic design criteria for new buildings." *Report No. NIST GCR 12-917-20*, prepared by the NEHRP Consultants Joint Venture for the National Institute of Standards and Technology, Gaithersburg, MD.

NZS (2007). "Steel structures standard, incorporating amendments No. 1 and No. 2." *NZS 3404*, Standards New Zealand, Wellington, New Zealand.

Pei, S. and van de Lindt, J. W. (2009). "Methodology for earthquake-induced loss estimation: An application to woodframe buildings." *Structural Safety*, 31(1), 31–42.

Porter, K. A., Kiremidjian, A. S., and LeGrue, J. S. (2001). "Assembly-based vulnerability of buildings and its use in performance evaluation." *Earthquake Spectra*, 17(2), 291–312.

Porter, K. A., Scawthorn, C. R., and Beck, J. L. (2006). "Cost-effectiveness of stronger woodframe buildings." *Earthquake Spectra*, 22(1), 239–266.

Ramirez, C. M., Liel, A. B., Mitrani-Reiser, J., Haselton, C. B., Spear, A. D., Steiner, J., Deierlein, G. G., and Miranda, E. (2012). "Expected earthquake damage and repair costs in reinforced concrete frame buildings." *Earthquake Engineering & Structural Dynamics*, 41(11), 1455–1475.

Ramirez, C. M. and Miranda, E. (2012). "Significance of residual drifts in building earthquake loss estimation." *Earthquake Engineering & Structural Dynamics*, 41(11), 1477–1493.

Ray-Chaudhuri, S. and Hutchinson, T. C. (2011). "Effect of nonlinearity of frame buildings on peak horizontal floor acceleration." *Journal of Earthquake Engineering*, 15(1), 124–142.

Rodriguez, M. E., Restrepo, J. I., and Carr, A. J. (2002). "Earthquake-induced floor horizontal accelerations in buildings." *Earthquake Engineering & Structural Dynamics*, 31(3), 693–718.

Roeder, C. W., Lumpkin, E. J., and Lehman, D. E. (2011). "A balanced design procedure for special concentrically braced frame connections." *Journal of Constructional Steel Research*, 67(11), 1760–1772.

Roeder, C. W., Lumpkin, E. J., and Lehman, D. E. (2012). "Seismic performance assessment of concentrically braced steel frames." *Earthquake Spectra*, 28(2), 709–727.

RS Means (2013). *RS Means Square Foot Costs*. RS Means Corp., Kingston, MA. USA.

Song, R., Li, Y., and van de Lindt, J. W. (2016). "Loss estimation of steel buildings to earthquake mainshockaftershock sequences." *Structural Safety*, 61, 1–11.

Stoakes, C. D. and Fahnestock, L. A. (2011). "Cyclic flexural testing of concentrically braced frame beam-column connections." *Journal of Structural Engineering*, 137(7), 739–747.

Storie, L. B., Pender, M. J., Clifton, G. C., and Wotherspoon, L. M. (2014). "Soil-foundation-structure interaction for buildings on shallow foundations in the Christchurch earthquake." *Proceedings of tenth U.S. National Conference on Earthquake Engineering Frontiers of Earthquake Engineering (10NCEE)*, Anchorage, AK.

Tremblay, R. (2002). "Inelastic seismic response of steel bracing members." *Journal of Constructional Steel Research*, 58(5-8), 665–701.

Tremblay, R., Filiatrault, A., Bruneau, M., Nakashima, M., Prion, H. G. L., and DeVall, R. (1996). "Seismic design of steel buildings: lessons from the 1995 Hyogo-ken Nanbu earthquake." *Canadian Journal of Civil Engineering*, 23(3), 727–756.

Tremblay, R., Filiatrault, A., Timler, P., and Bruneau, M. (1995). "Performance of steel structures during the 1994 Northridge earthquake." *Canadian Journal of Civil Engineering*, 22(2), 338–360.

Vamvatsikos, D. and Cornell, C. A. (2002). "Incremental dynamic analysis." *Earthquake Engineering & Structural Dynamics*, 31(3), 491–514.

Zareian, F. and Kanvinde, A. (2013). "Effect of column-base flexibility on the seismic response and safety of steel moment-resisting frames." *Earthquake Spectra*, 29(4), 1537–1559.

List of Tables

TABLE 1 Dual-parameter fragility distribution functions for steel braces (Lignos and Karamanci 2013)

Assembly description	Damage state[a]	Fragility parameters					
		μ_{SDR} (%)	$\beta_{\ln SDR}$	$\mu_{KL/r}$	$\beta_{\ln kL/r}$	$\mu_{(D/t)/\lambda_{hd}^{b}}$	$\beta_{\ln(D/t)/\lambda_{hd}^{b}}$
Round HSS Braces	DS1	0.41	0.51	63.6	0.46	0.97	0.47
	DS2	0.96	0.45	66.1	0.45	1.02	0.42
	DS3	2.75	0.51	68.9	0.40	1.11	0.33

[a] DS1 = global buckling; DS3 = local buckling; and DS3 = brace fracture.

[b] λ_{hd} = the corresponding seismic compactness limit specified in AISC (2010).

TABLE 2 Fragility and cost estimates for steel-frame buildings with perimeter SCBFs

Assembly description	Damage state[a]	Unit	Fragility parameters			Repair cost parameters
			EDP[b]	x_m^c	β^d	x_m^c ($)
Columns base (W $< 223 kg/m$) (FEMA 2012)	Crack initiation	EA	SDR	0.04	0.40	19224
	Crack propagation			0.07	0.40	27263
	Fracture			0.10	0.40	32423
Columns base ($223 kg/m <$ W $\leq 446 kg/m$) (FEMA 2012)	Crack initiation	EA	SDR	0.04	0.40	20082
	Crack propagation			0.07	0.40	29395
	Fracture			0.10	0.40	36657
Columns base (W$> 446 kg/m$) (FEMA 2012)	Crack initiation			0.04	0.40	21363
	Crack propagation	EA	SDR	0.07	0.40	32567
	Fracture			0.10	0.40	41890
Column splices (W$< 223 kg/m$) (FEMA 2012)	Crack initiation	EA	SDR	0.04	0.40	9446
	Crack propagation			0.07	0.40	11246
	Fracture			0.10	0.40	38473
Column splices ($223 kg/m <$ W $\leq 446 kg/m$) (FEMA 2012)	Crack initiation	EA	SDR	0.04	0.40	10246
	Crack propagation			0.07	0.40	13012
	Fracture			0.10	0.40	42533
Column splices (W $> 446 kg/m$) (FEMA 2012)	Crack initiation	EA	SDR	0.04	0.40	11446
	Crack propagation			0.07	0.40	14812
	Fracture			0.10	0.40	47594
Column ($\leq$ W27) (FEMA 2012)	LB	EA	SDR	0.03	0.30	16033
	LTB			0.04	0.30	25933
	Fracture			0.05	0.30	25933
Column ($\geq$ W30) (FEMA 2012)	LB	EA	SDR	0.03	0.30	17033
	LTB			0.04	0.30	28433
	Fracture			0.05	0.30	28433
Rectangular HSS (Brace weight $< 60 kg/m$) (Lignos and Karamanci 2013)	GB	EA	SDR	0.40	0.43	29983
	LB			1.02	0.44	37014
	Brace Fracture			1.60	0.48	36480
Rectangular HSS ($61 kg/m <$ Brace weight $< 147 kg/m$) (Lignos and Karamanci 2013)	GB	EA	SDR	0.40	0.43	29983
	LB			1.02	0.44	47115
	Brace Fracture			1.60	0.48	47882

TABLE 2 Fragility and cost estimates for steel-frame buildings with perimeter SCBFs (continued)

Assembly description	Damage state[a]	Unit	Fragility parameters			Repair cost parameters
			EDP[b]	x_m^c	β^d	x_m^c ($)
Round HSS (Brace weight $< 60kg/m$) (Lignos and Karamanci 2013)	GB	EA	SDR	0.41	0.51	29983
	LB			0.96	0.45	37014
	Brace Fracture			2.75	0.51	36480
Round HSS ($61kg/m <$ Brace weight $< 147kg/m$) (Lignos and Karamanci 2013)	GB	EA	SDR	0.41	0.51	29983
	LB			0.96	0.45	47115
	Brace Fracture			2.75	0.51	47882
Moment connections (one-sided, $\leq$ W27) (FEMA 2012)	LB	EA	SDR	0.03	0.30	16033
	LTB			0.04	0.30	25933
	Fracture			0.05	0.30	25933
Moment connections(one-sided, $\geq$ W30) (FEMA 2012)	LB	EA	SDR	0.03	0.30	17033
	LTB			0.04	0.30	28433
	Fracture			0.05	0.30	28433
Moment connections (two-sided, $\leq$ W27) (FEMA 2012)	LB	EA	SDR	0.03	0.30	30400
	LTB			0.04	0.30	47000
	Fracture			0.05	0.30	47000
Moment connections (two-sided, $\geq$ W30) (FEMA 2012)	LB	EA	SDR	0.03	0.30	30400
	LTB			0.04	0.30	52399
	Fracture			0.05	0.30	52399
Shear tab connections (FEMA 2012)	Yielding	EA	SDR	0.04	0.40	12107
	Partial tearing			0.08	0.40	12357
	Complete separation			0.11	0.40	12307
Corrugated slab ($90mm$ steel; $100mm$ overlay) (Hwang et al. 2015)	Crack initiations	m^2	SDR	0.00375	0.13	180
	Crushing near column			0.01	0.22	330
	Shear stud fracture			0.05	0.35	570
Drywall partition (Ramirez et al. 2012)	Visible	$6m^2$	SDR	0.0039	0.17	90
	Significant			0.0085	0.23	530
Drywall finish (Ramirez et al. 2012)	Visible	$6m^2$	SDR	0.0039	0.17	90
	Significant			0.0085	0.23	250
Exterior glazing (Ramirez et al. 2012)	Crack	pane	SDR	0.04	0.36	440
	Fallout			0.046	0.33	440
Suspended ceiling ($A > 232m^2$) (FEMA 2012)	5% tiles dislodge	$232m^2$	PFA(g)	0.35	0.40	3542
	30% tiles dislodge			0.55	0.40	29337
	Collapse			0.80	0.40	55200

TABLE 2 Fragility and cost estimates for steel-frame buildings with perimeter SCBFs (continued)

Assembly description	Damage state[a]	Unit	Fragility parameters			Repair cost parameters
			EDP[b]	x_m^{c}	β^{d}	x_m^{c} ($)
Automatic sprinklers (Ramirez et al. 2012)	Fracture	3.66m	PFA(g)	0.32	1.40	900
Elevator (FEMA 2012)	Failure	EA	PGA(g)	0.50	0.28	868

[a]GB=Global buckling, LB=local buckling, LTB=lateral-torsional buckling.

[b]SDR=story drift ratio, PFA=peak floor acceleration (g), PGA=peak ground acceleration (g).

[c] x_m=median value of assembly fragility curve.

[d]β=lognormal standard deviation.

TABLE 3 Median and logarithmic standard deviation of collapse fragility curves for all the analytical model representations of the archetype steel buildings with SCBFs

	$\hat{S}_{CT}(T_1, 5\%)/g$				β_{RTR}			
	SDC D_{max}		SDC D_{min}		SDC D_{max}		SDC D_{min}	
No. of stories	*B*	*CG*	*B*	*CG*	*B*	*CG*	*B*	*CG*
2	2.96	3.75	1.30	1.90	0.48	0.48	0.56	0.54
3	4.22	4.31	1.76	1.90	0.50	0.54	0.56	0.61
6	2.51	3.09	1.34	1.73	0.59	0.48	0.60	0.58
12	1.11	1.68	0.71	1.23	0.73	0.63	0.50	0.53

TABLE 4 Normalized EALs for archetype buildings with SCBFs based on drift-based steel brace fragility curves

Building model		Replacement cost (millions U.S. dollars)	EAL (%) nonstructural losses Acc	nonstructural losses Drift	Structural losses	Demolition losses	Collapse losses	Total losses
SDC D_{max}								
2	*B*	7.56	0.623	0.020	0.061	0.092	0.020	0.816
	CG		0.690	0.022	0.068	0.012	0.009	0.801
3	*B*	11.34	0.648	0.027	0.049	0.011	0.004	0.738
	CG		0.707	0.025	0.047	0.008	0.005	0.792
6	*B*	22.68	0.663	0.049	0.071	0.034	0.015	0.832
	CG		0.666	0.043	0.061	0.013	0.005	0.788
12	*B*	45.36	0.562	0.063	0.159	0.045	0.043	0.872
	CG		0.623	0.044	0.113	0.006	0.015	0.801
SDC D_{min}								
2	*B*	7.56	0.315	0.012	0.040	0.005	0.020	0.392
	CG		0.395	0.013	0.037	0.000	0.005	0.450
3	*B*	11.34	0.521	0.015	0.036	0.001	0.003	0.577
	CG		0.594	0.015	0.035	0.000	0.004	0.647
6	*B*	22.68	0.334	0.035	0.059	0.002	0.002	0.432
	CG		0.419	0.029	0.051	0.000	0.001	0.501
12	*B*	45.36	0.395	0.044	0.132	0.005	0.001	0.577
	CG		0.435	0.029	0.090	0.001	0.000	0.556

Note that all values in the table are expressed as a percentage of the total replacement cost of the respective building

List of Figures

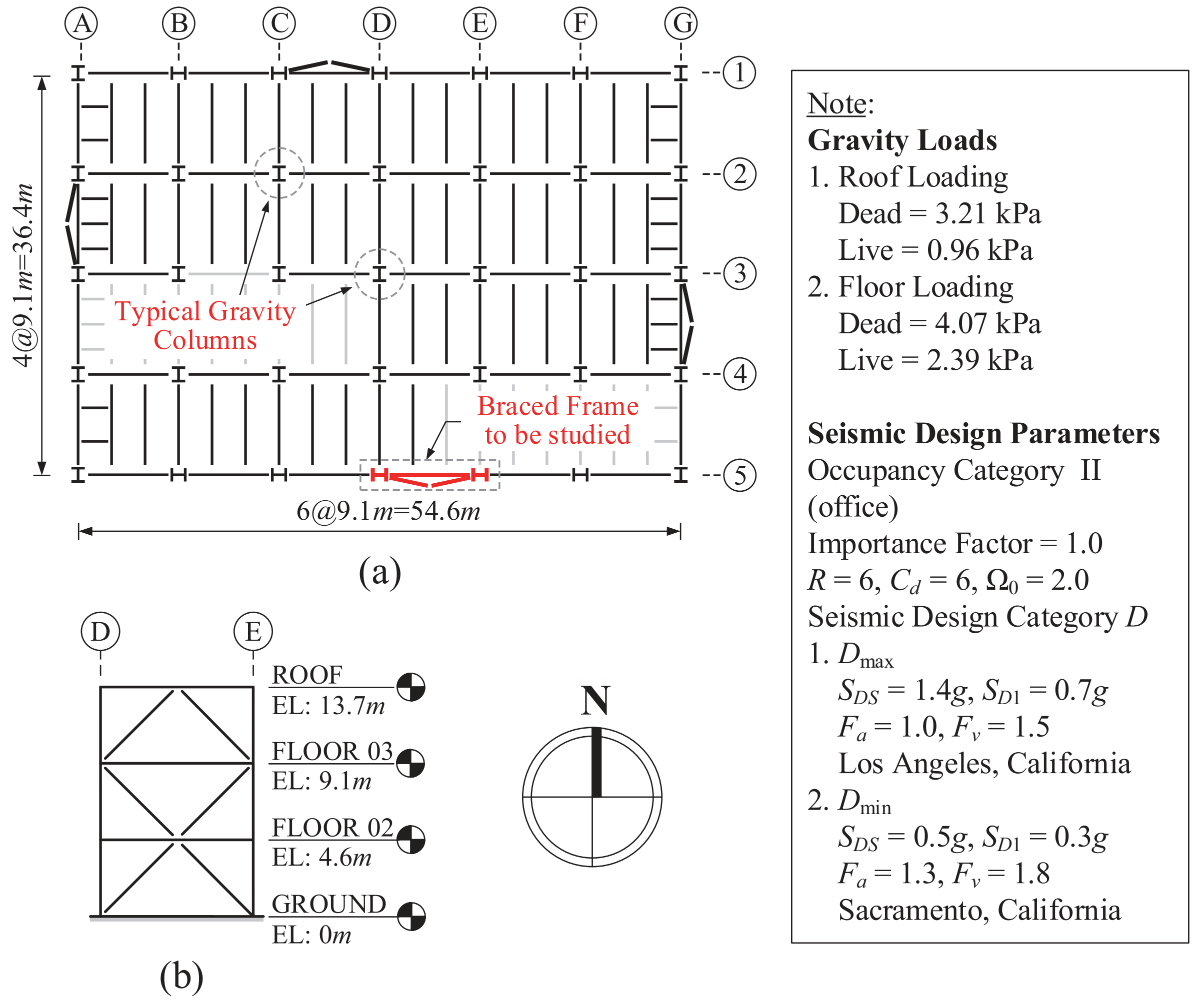

FIG. 1 Archetype steel-frame buildings with perimeter SCBFs: (a) typical plan view; and (b) elevation view of the 3-story SCBF

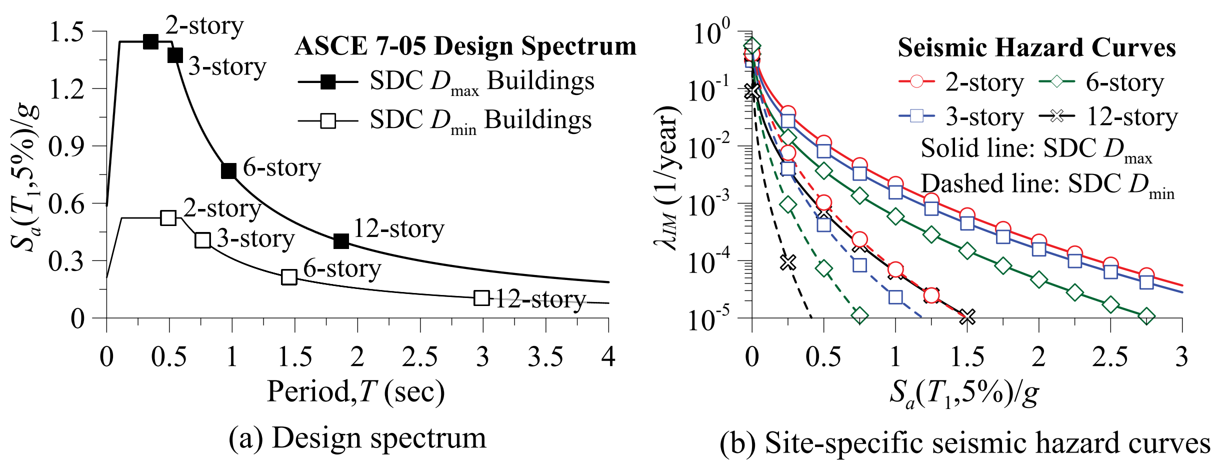

FIG. 2 Design spectrum and site-specific seismic hazard curves for bare model representations of archetype buildings with SCBFs

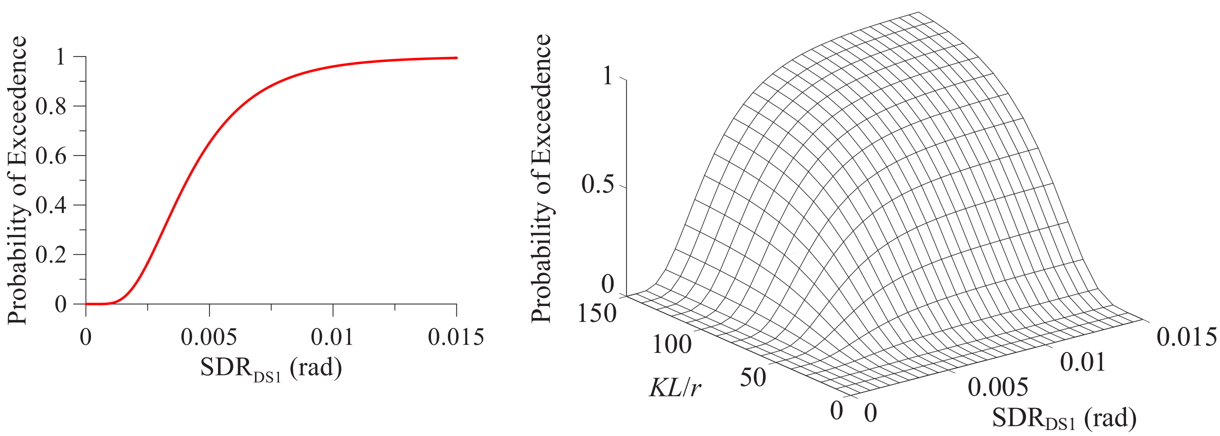

(a) Univariate fragility curve (b) Dual-parameter fragility curve

FIG. 3 Example of fragility curves for damage state of global buckling for round HSS braces: (a) univariate fragility curve; and (b) dual-parameter (global slenderness KL/r) fragility curves [adopted from Lignos and Karamanci (2013)]

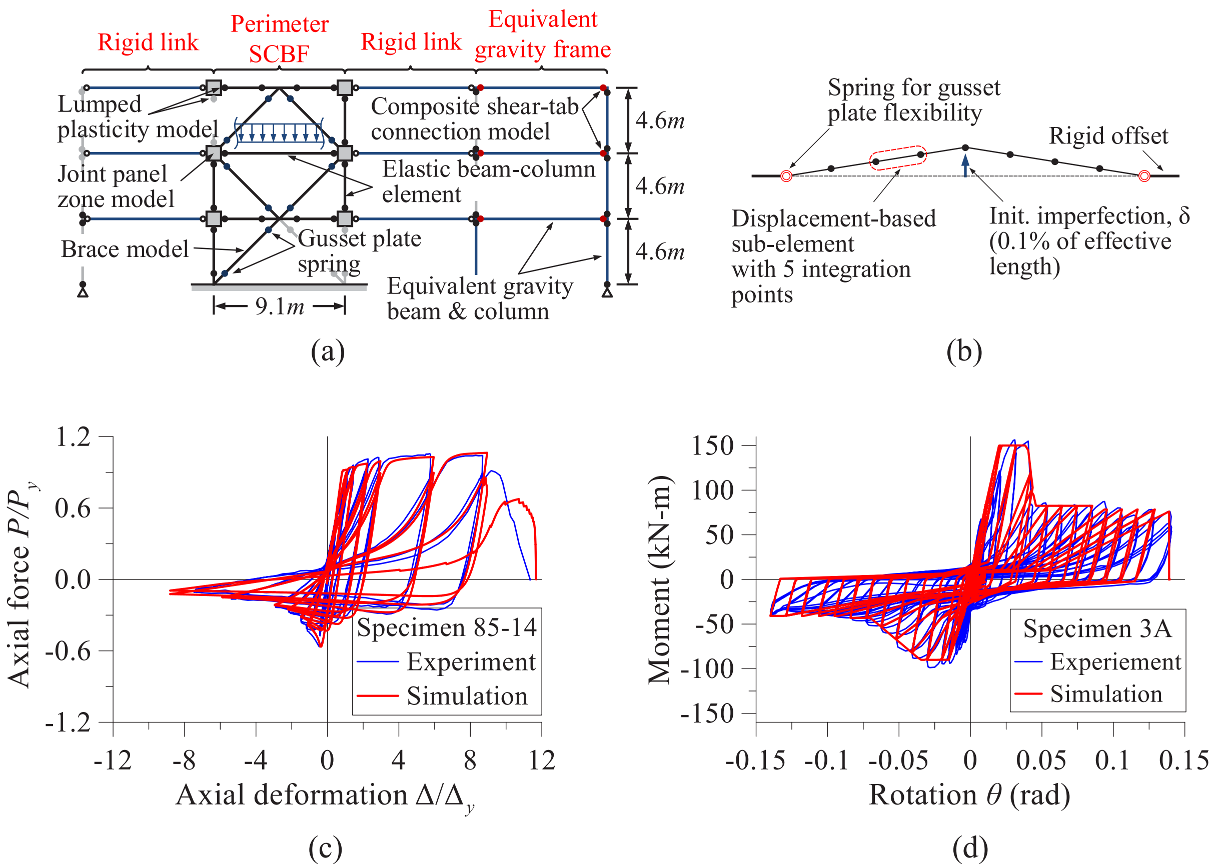

FIG. 4 Analytical model representation of steel-frame buildings with SCBFs: (a) 2-D analytical model including the gravity framing (CG model); (b) description of the steel brace component model; (c) axial force-deformation relation for rectangular HSS brace section [data from Han et al. (2007)]; and (d) moment-chord rotation relation for composite beam in single-plate shear tab connections [data from Liu and Astaneh-Asl (2000)]

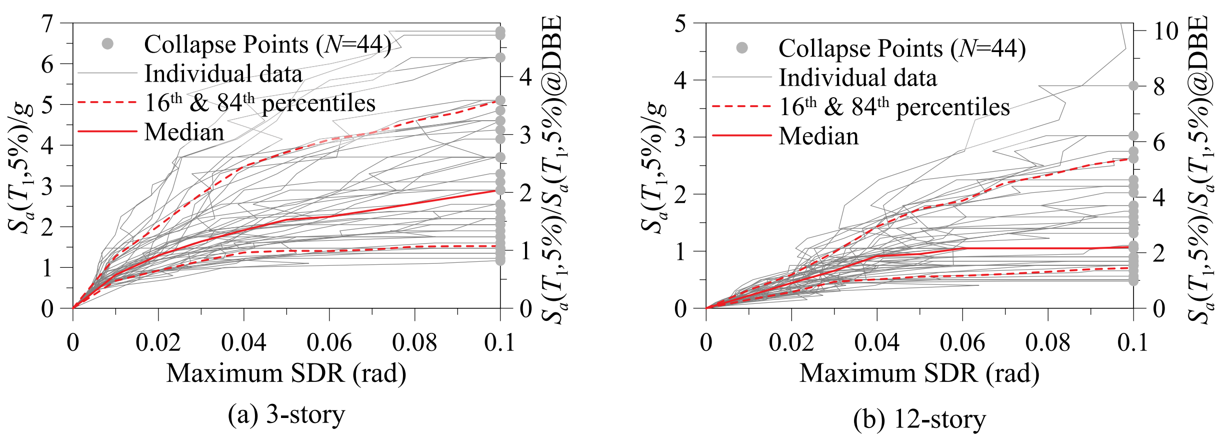

FIG. 5 IDA curves for the 3- and 12-story steel-frame buildings with perimeter SCBFs (CG models)

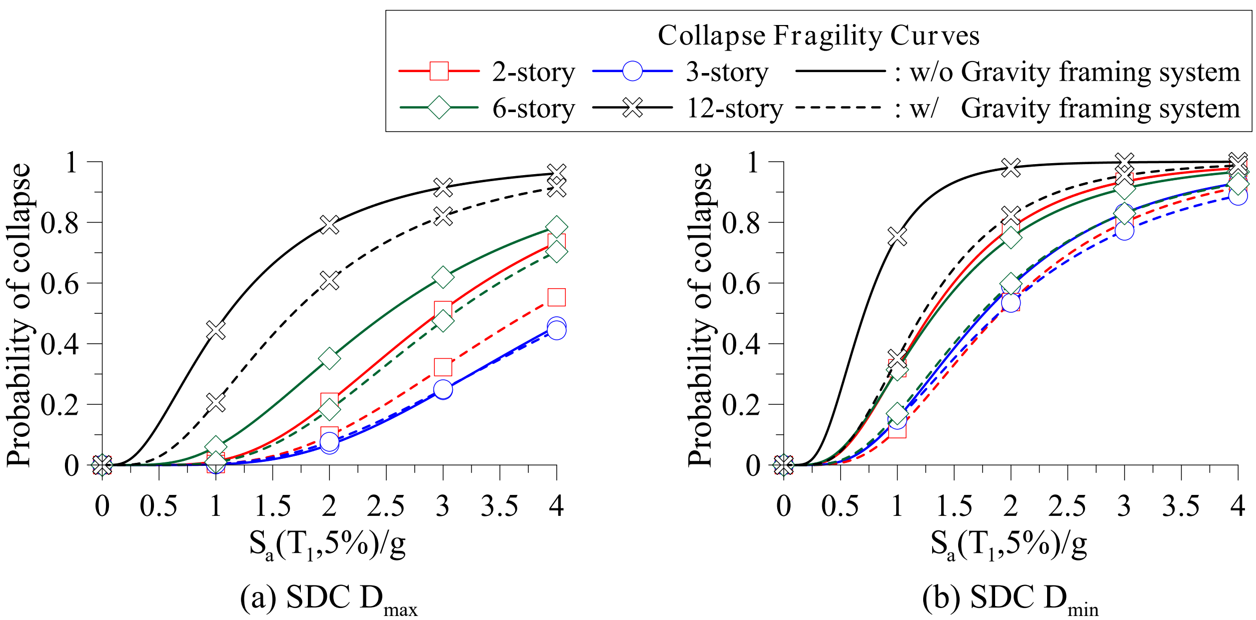

FIG. 6 Collapse fragility curves for steel-frame buildings with perimeter SCBFs with/without gravity framing system

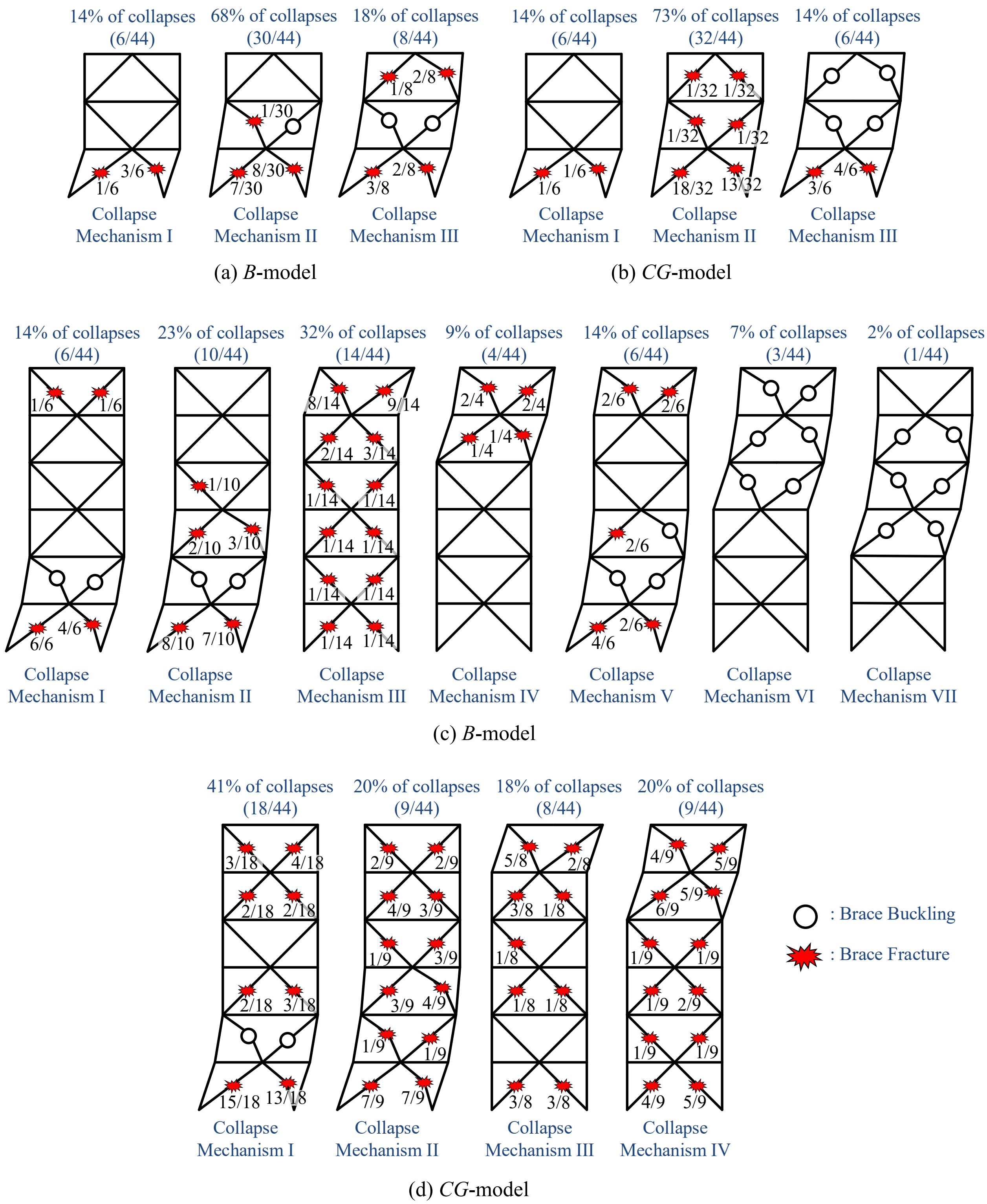

FIG. 7 Collapse mechanisms for the 3- and 6-story archetypes based on B and CG models

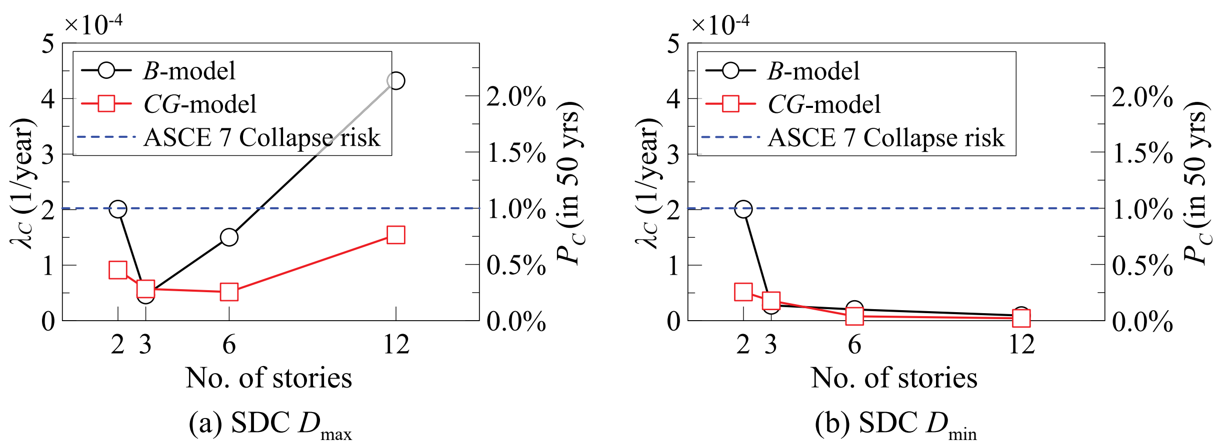

FIG. 8 Mean annual frequency of collapse λ_c and the corresponding collapse probability over 50 years P_c (in 50 years) for the analytical model type of archetype buildings with perimeter SCBFs

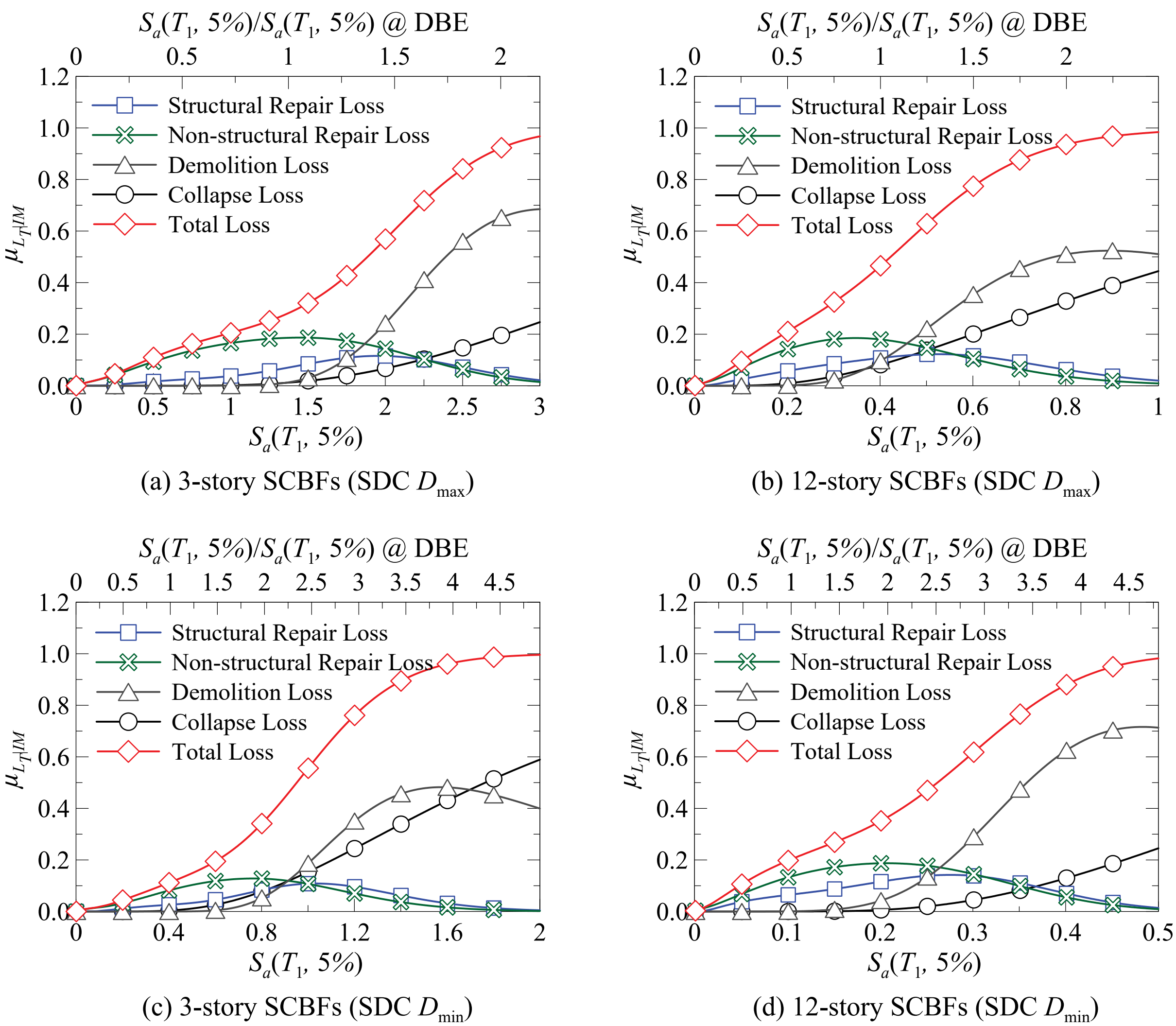

FIG. 9 Normalized loss vulnerability curves for steel-frame buildings with perimeter SCBFs designed for SDC D_{max} and D_{min} conditioned on seismic intensity

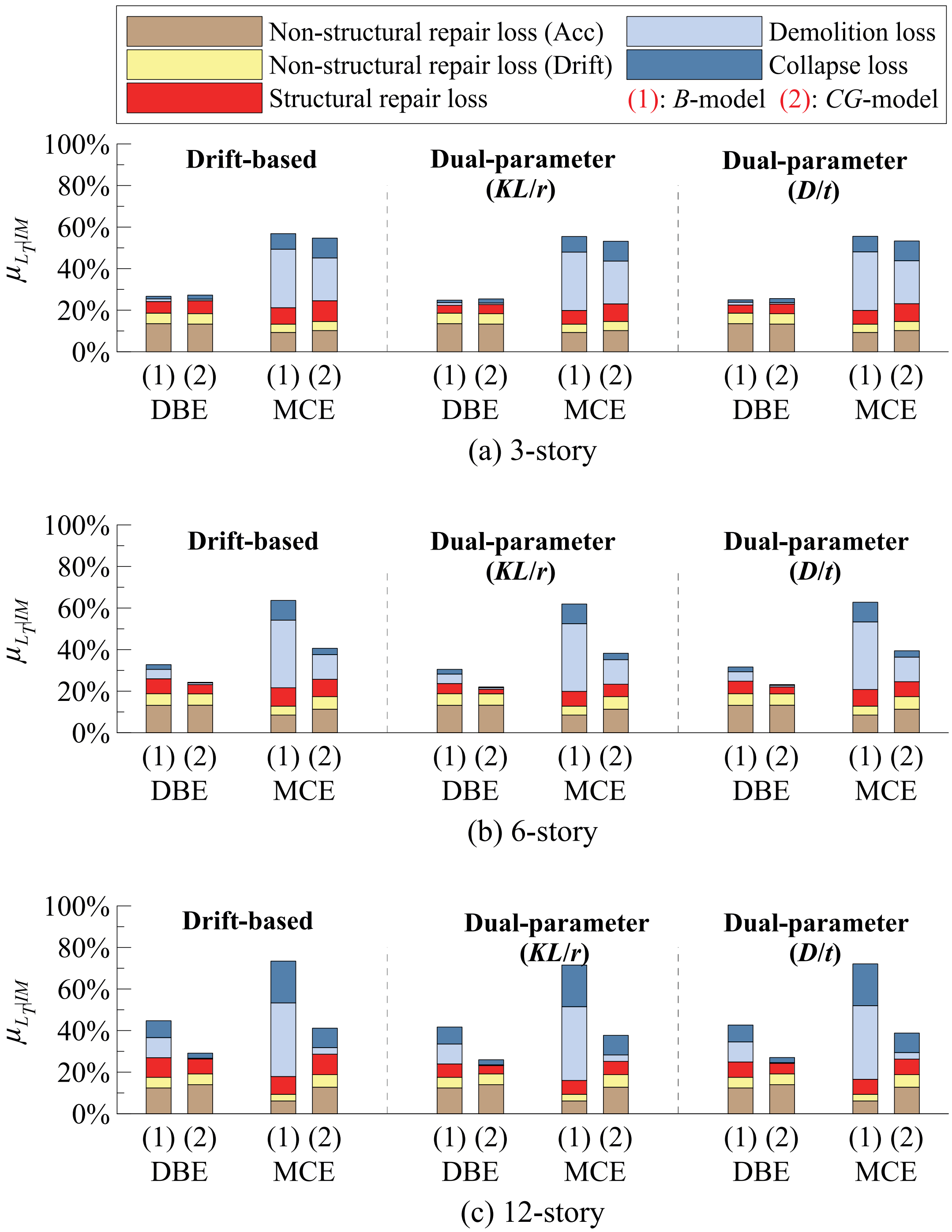

FIG. 10 Normalized expected losses of steel-frame buildings with perimeter SCBFs designed for SDC D_{max} conditioned on selected seismic intensities

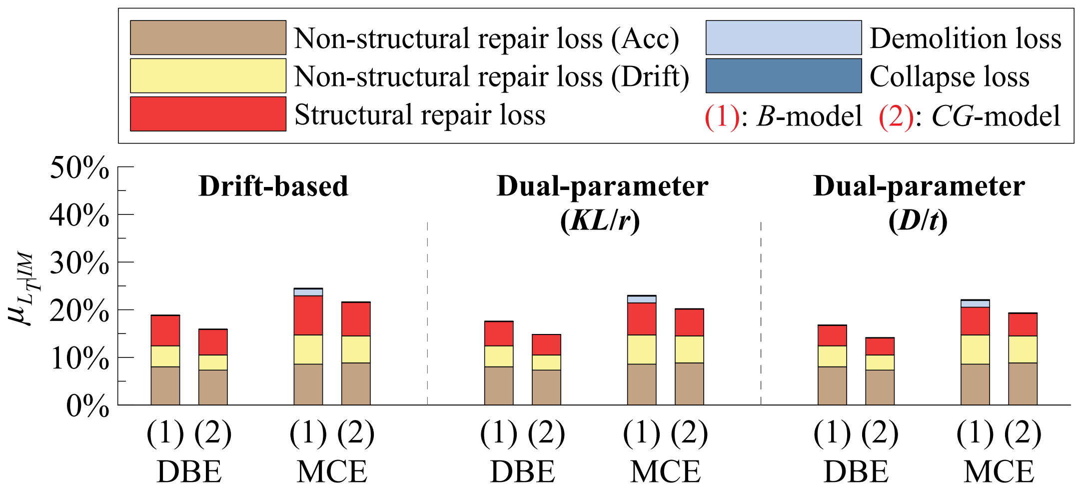

FIG. 11 Normalized expected losses of the 12-story steel-frame building with perimeter SCBFs designed for SDC D_{min} conditioned on selected seismic intensities

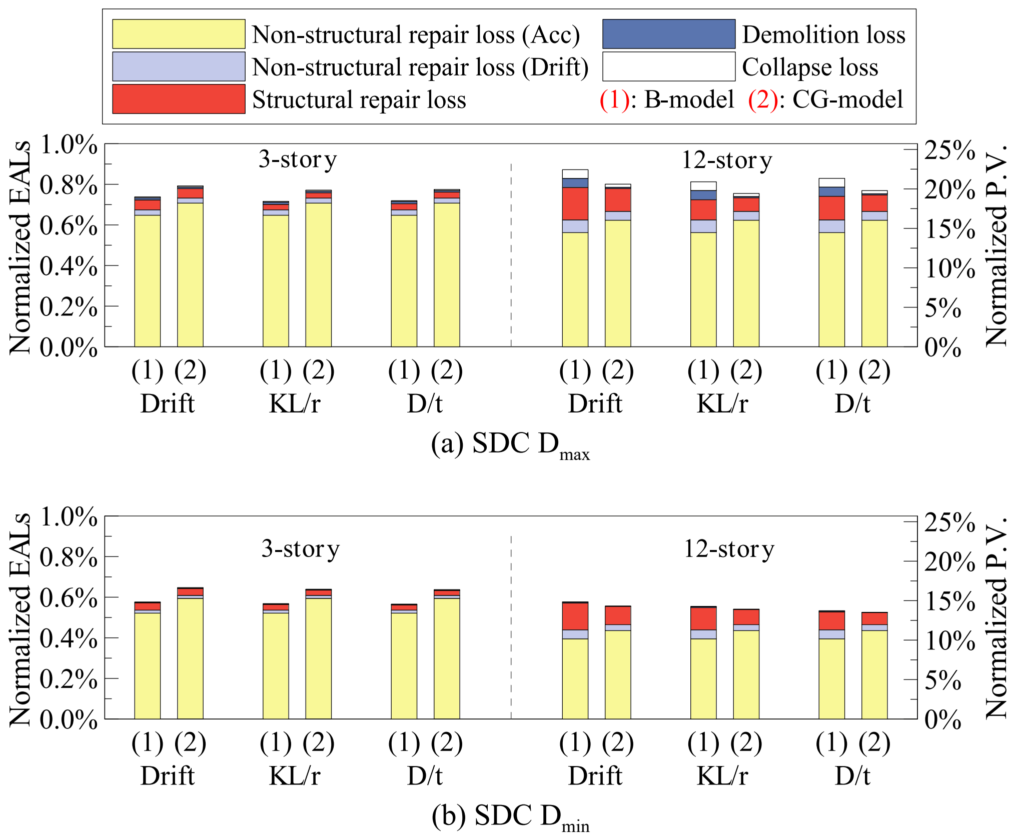

FIG. 12 Normalized expected annual losses and present values for steel-frame buildings with SCBFs